12

STOCHASTIC METHODS FOR MAGNETIC RESONANCE SPECTROSCOPIES

ANTONINO POLIMENO

Dipartimento di Scienze Chimiche, Università degli Studi di Padova, Padova, Italy

VINCENZO BARONE

Scuola Normale Superiore di Pisa, Pisa, Italy

JACK H. FREED

Department of Chemistry and Chemical Biology, Cornell University, Ithaca, New York

Computational Strategies for Spectroscopy: From Small Molecules to Nano Systems, First Edition. Edited by Vincenzo Barone.

Physicochemical properties of molecules in solution depend on the action of different motions at several time and length scales, and information on multiscale dynamics can be gained, in principle, by a variety of spectroscopic techniques. In this work we review theoretical tools for the investigation of "slow" molecular motions, such as solvent cage effects in liquids and liquid crystals, global and local dynamics in proteins, reorientation dynamics, and internal (conformational) degrees of freedom. Spectroscopic techniques which are most sensitive to such motions are electron spin resonance and nuclear magnetic resonance and they require ad hoc theoretical treatment. In particular, we discuss the definition of multidimensional stochastic models and their treatment to interpret magnetic resonance spectroscopic data of rigid and flexible molecules in isotropic media, liquid crystals, and biosystems.

12.1 INTRODUCTION

It is natural for a chemist to consider molecules as dynamical systems. Thermal effects and interactions with other molecules influence both internal and global molecular degrees of freedom. Macroscopic chemical and physical properties of molecules depend on their dynamics to varying degrees, based upon the physical observable considered. Examples of dynamical physical chemistry are numerous: Collision theory is based on the assumption that molecules move (in order to collide) to react; temperature is the macroscopic physical observable which is related to the average square velocity of particles; osmotic pressure in biological cells is kept at a fixed point value by the action of Na/K pumps, which are molecular machines that carry out their function due to internal dynamics; many enzymes can react and transform a substrate because of change of conformation that occurs in bonding, and this serves to create the right chemical environment around the substrate.

Thus interpretation of structural properties and dynamic behavior of molecules in solution is of fundamental importance to understand their stability, chemical reactivity, and catalytic action. Great interest exists in the development of new materials and the study of biological macromolecules. In general, one has to treat complex systems in which motions are present over a wide range of time scales encompassing global dynamics (microseconds), domain dynamics (nanoseconds), and localized fluctuations involving selected chemical groups (picoseconds to femtoseconds).

Given that a key role of theoretical chemistry is to interpret macroscopic observations in terms of physicochemical properties of molecules, dynamics is a fundamental ingredient as well as structure. This is especially true for models designed to interpret processes occurring in large biomolecules or complex ("soft") materials. In this work our main purpose is to review integrated theoretical/computational approaches for interpreting motions typically in the range 10^{-9}–10^{-6} s in complex molecular systems. We will refer to this range as slow molecular motions or just "slow motions". The main objective is the study of the dynamics (mobility) of complex systems, mainly of biomolecular interest, by means of the interpretation of spectroscopic data for obtaining information on their dynamics [1]. Indeed, information on dynamics can be inferred, in most cases, only indirectly

from experiments. A theoretical framework is therefore required to link macroscopic observations to molecular dynamics. A sensible plan of action is then to (i) choose a reference experimental technique which is particularly sensitive to the type of motions we are interested in; (ii) set up a framework for describing the dynamics and its influence on the chosen physical observable; and (iii) select model systems which serve to build and test theoretical models.

Experimental determination of dynamical properties of molecular systems is often based on sophisticated spectroscopic techniques. Given that the properties of molecules in solution result from motions at several time and length scales, insight on multiscale dynamics can be gained, in principle, by a range of spectroscopic techniques: magnetic [nuclear magnetic resonance (NMR) and electron spin resonance (ESR)] and optical [fluorescence polarization anisotropy (FPA), dynamic light scattering (DLS), and time-resolved Stokes shift (TRSS)]. In this review we focus on slow molecular motions (e.g., dynamic solvation effects, reorientation dynamics, conformational dynamics) monitored by magnetic spectroscopies, both ESR and NMR. In the case of ESR, this means that slow-motion processes have characteristic time scales that are comparable to those of electronic spin relaxation.

This contribution reviews the basic tools which are currently employed for interpreting ESR and NMR observables in condensed phases, with an emphasis on stochastic modeling as key for the prediction of continuous-wave ESR (cw-ESR) lineshapes and NMR relaxation times of proteins. Section 12.2 is therefore devoted to the definition of reduced (effective) magnetic Hamiltonians and the stochastic (Liouville) approach to spin/molecular dynamics in order to clarify the basic stochastic approach to cw-ESR observables. Section 12.3 provides a short overview of rotational stochastic models for the evaluation of relaxation NMR data in biomolecules. Conclusions are briefly summarized in Section 12.4.

12.2 MODELING A cw-ESR EXPERIMENT

Magnetic resonance spectroscopies and theoretical chemistry have always been linked. On the one hand, the rich and detailed information hidden in ESR and NMR spectra has been a challenge for physicochemical interpretations and computational models. On the other hand, magnetic resonance spectroscopists have been looking for better tools to interpret the spectra.

12.2.1 ESR: Modeling and Observables

The intrinsic resolution of ESR spectra together with the unique role played by paramagnetic probes in providing information on their environment makes ESR one of the most powerful methods of investigation of electronic distributions in molecules and the properties of their environments. The theoretical tools needed by ESR spectroscopists come from quantum chemistry to provide the parameters of the spin Hamiltonian appropriate for room temperature (experiments usually can supply them

but for frozen solutions at low temperatures) and from molecular dynamics and statistical mechanics for the spectral lineshapes.

Because of their favorable time scales, ESR experiments can be very sensitive to the details of the rotational and internal dynamics. In particular, with the advent of very high field ESR corresponding to frequencies at and above 140 GHz, the rotational dynamics of spin-labeled molecules observed by ESR is more commonly found to be in the so-called slow-motion regime than is the case at conventional ESR frequencies (e.g., 9.5 GHz) [2]. For this regime, the spectral lineshapes take on a complex form which is found to be sensitive to the microscopic details of the motional process [2]. This is to be contrasted with the fast-motion regime, where simple Lorentzian lineshapes are observed, and only estimates of molecular parameters (e.g., diffusion tensor values) are obtained independently from the microscopic details of the molecular dynamics. The interpretation of slow-motion spectra requires an analysis based upon sophisticated theory, as will be emphasized in the next section. ESR spectroscopy is applied extensively to materials science and to biochemistry. Great interest is focused particularly on the study of the dynamics of biological molecules, such as proteins and, in particular, ESR studies of proteins via site-directed spin labeling (SDSL) with stable nitroxide radicals [3–6]. The wealth of dynamic information which can be extracted from a cw-ESR or an electron–electron double-resonance (ELDOR) spectrum with nitroxide labels is at present limited experimentally by the challenge of obtaining extensive multifrequency data [6] and theoretically by the necessity of employing computationally efficient dynamic models [2, 7–9]. The review of Borbat et al. [10] provides a discussion of modern ESR techniques for studying basic molecular mechanisms in proteins and membranes by using nitroxide spin labels. These include the direct measurement of distances in biomolecules and unraveling the details of complex molecular dynamics. These studies can, for instance, provide information on phospholipid membranes [11–14] which can be described via augmented stochastic models. Since the relationship between ESR spectroscopic measurements and most molecular properties can be obtained only indirectly via modeling and numerical simulations one may utilize the spectroscopic data as the "target" of a fitting procedure of molecular, mesoscopic, and macroscopic parameters entering the model.

An intrinsic limitation of this approach is the difficulty of avoiding uncertainties due to multiple minima in the fitting procedure and the difficulty, in many cases, to reconcile best-fit parameters with more general approaches or known physical trends (e.g., temperature dependence).

A more refined methodology is based on an integrated computational approach, that is, the combination of (i) quantum mechanical (QM) calculations of structural parameters and magnetic tensors possibly including average interactions with the environment (by discrete–continuum models) and short-time dynamical effects; (ii) direct feeding of calculated molecular parameters into dynamic models based on molecular dynamics and coarse-grain dynamics; and, above all, (iii) stochastic modeling. Fine tuning of a limited set of molecular or mesoscopic parameters via limited fitting can still be employed. In particular, ESR measurements are becoming particularly amenable to an integrated approach, due to increasing experimental

progress, advancement in computational methods, and refinement of available dynamical models.

Nitroxide-derived paramagnetic probes allow in principle the detection of several types of information at once: secondary-structure information, interresidual distances, if more than one spin probes is present, and large-amplitude protein motions from the overall ESR spectrum shape [15–19]. An ab initio interpretation of ESR spectroscopy needs to take into account different aspects regarding the structural, dynamical, and magnetic properties of the molecular system under investigation, and it requires, as input parameters, the known basic molecular information and solvent macroscopic parameters. The application of the stochastic Liouville equation formalism integrates the structural and dynamic ingredients to give directly the spectrum with minimal additional fitting procedures in the presence of internal dynamics, anisotropic environments, and so on [2, 20–27] Notice that alternative computational treatments of multifrequency ESR signals are nowadays emerging. In particular, standard molecular dynamics–based approaches [28] have been employed recently, and novel augmented treatments are being developed [29].

Properties of liquid crystals as order parameters, dynamics, and cage effects have been studied by several authors using ESR spectroscopy of dissolved spin probes and a stochastic Liouville equation (SLE)–based approach for interpretation. For instance, Sastry and co-workers [7, 8] studied two-dimensional Fourier transform (2D-FT) ESR of the rigid rodlike cholestane (CSL) spin label in the liquid crystal solvent butoxy benzylidene octylaniline (4O,8) and the small globular spin probe perdeuterated tempone (PDT) in the same solvent. Experimental spectra were collected over a wide range of temperatures in such a way as to include isotropic, nematic, smectic A and B, and crystal phases of 4O,8. 2D-FT-ESR was chosen because it provides greatly enhanced sensitivity to rotational dynamics over cw-ESR analysis. For both the CSL and PDT spin probes, experimental spectra were interpreted via the slowly relaxing local structure (SRLS) model [30] in which the dynamic of the system is described with two coupled relaxing processes which are interpreted as a fast global tumbling of the probe and a slow relaxation of the solvent cage collective motions. Zannoni and co-workers [31] used the ESR spin probe technique to study the changes in phase stability, orientational order, and dynamics of the nematic 5-cyanobiphenyl (5CB) doped with different cis/trans *p*-azobenzene derivatives. CSL was again adopted as the spin probe to monitor the order and the dynamics of the liquid crystal system, owing to its size, rigidity, and rodlike shape analogous to that of the 5CB [32–34]. Interpretation of the experimental spectra was carried out by simulations with the one-body model implementation by Freed [35] by assuming the probe as a rigid rotator that reorients under the action of a second-rank potential.

The theoretical approach to the interpretation of ESR spectra is based on the solution of the SLE. This is essentially a semiclassical approach based on the Liouville equation for the magnetic probability density of the molecule augmented by a stochastic operator which describes the relevant relaxation processes that occur in the system and is responsible for the broadening of the spectral lines [2]. The SLE approach can be linked profitably to density functional theory (DFT) evaluation of geometry and magnetic parameters of the radical in its

environment. Dissipative parameters, such as rotational diffusion tensors, can in turn be determined at a coarse-grained level by using standard hydrodynamic arguments. The combination of the evaluation of structural properties, based on quantum mechanical advanced methods, with hydrodynamic modeling for dissipative properties and, in the case of multilabeled systems, determination of dipolar interaction based on the molecular structures beyond the point approximation are the fundamental ingredients needed by the SLE to provide a fully integrated computational approach (ICA) that gives the spectral profile. A number of parameters enter in the definition of the SLE and customarily a multicomponent fitting procedure is employed. ICA attempts to replace fitting procedures as much as possible with the ab initio evaluation of parameters in order to give them a sound physical interpretation, and fitting may be retained as a "refining" step. The calculation of ESR observables can in principle be based on the complete solution of the Schrödinger equation for the system made of paramagnetic probe + explicit solvent molecules. The system can be described by a "complete" Hamiltonian $\hat{H}(\mathbf{r}_i, \mathbf{R}_k, \mathbf{q}_\alpha)$, which can be written in the form

$$\hat{H}(\mathbf{r}_i, \mathbf{R}_k, \mathbf{q}_\alpha) = \hat{H}_{\text{probe}}(\mathbf{r}_i, \mathbf{R}_k) + \hat{H}_{\text{probe-solvent}}(\mathbf{r}_i, \mathbf{R}_k, \mathbf{q}_\alpha) + \hat{H}_{\text{solvent}}(\mathbf{q}_\alpha) \quad (12.1)$$

where probe and solvent terms are separated. The Hamiltonian $\hat{H}(\mathbf{r}_i, \mathbf{R}_k, \mathbf{q}_\alpha)$ contains (i) electronic coordinates $\mathbf{r}_i$, of the paramagnetic probe (where index i runs over all probe electrons), (ii) nuclear coordinates $\mathbf{R}_k$ (where index k runs over all rotovibrational nuclear coordinates), and (iii) coordinates $\mathbf{q}_\alpha$, in which we include all degrees of freedom of the solvent molecules, each labeled by index α. The basic object of study, to which any spectroscopic observable can be linked, is given by the density matrix $\hat{\rho}(\mathbf{r}_i, \mathbf{R}_k, \mathbf{q}_\alpha)$, which in turn is obtained from the Liouville equation

$$\frac{\partial \hat{\rho}}{\partial t} = -\frac{i}{\hbar}[\hat{H}, \hat{\rho}] = -i\hat{\mathcal{L}}\hat{\rho} \quad (12.2)$$

Solving Eq. 12.2 in time—for instance, via an ab initio molecular dynamics scheme—allows in principle the direct evaluation of the density matrix and hence calculation of any molecular property [29]. However, significant approximations are possible which are basically rooted in time-scale separation. The nuclear coordinates $\mathbf{R} \equiv \mathbf{R}_k$ can be separated into fast-probe vibrational coordinates $\mathbf{R}_{\text{fast}}$ from slow-probe coordinates, that is, rotational and intramolecular "soft" torsional degrees of freedom, $\mathbf{Q}$, relaxing at least in a picosecond time scale. Then the probe Hamiltonian is averaged on (i) femtosecond and subpicosecond dynamics pertaining to probe electronic coordinates and (ii) picosecond dynamics pertaining to probe internal vibrational degrees of freedom. The averaging over the electron coordinates is the usual implicit procedure for obtaining a spin Hamiltonian from the complete Hamiltonian of the radical. In the frame of a Born–Oppenheimer approximation, the averaging over the picosecond dynamics of nuclear coordinates allows one to introduce in the calculation of magnetic parameters the effect of vibrational motion. In this way a probe Hamiltonian is obtained characterized by magnetic tensors. By taking into account only the electron Zeeman and the hyperfine interactions, for a

probe with one unpaired electron and N nuclei, we can define an averaged magnetic Hamiltonian $\hat{H}(\mathbf{Q}, \mathbf{q}_\alpha)$:

$$\hat{H}(\mathbf{Q}, \mathbf{q}_\alpha) = \frac{\beta_e}{\hbar}\mathbf{B}_0\mathbf{g}(\mathbf{Q}, \mathbf{q}_\alpha)\hat{\mathbf{S}} + \gamma_e \sum_n \hat{\mathbf{I}}_n \mathbf{A}_n(\mathbf{Q}, \mathbf{q}_\alpha)\hat{\mathbf{S}} + \hat{H}_{\text{probe-solvent}}(\mathbf{Q}, \mathbf{q}_\alpha) + \hat{H}_{\text{solvent}}(\mathbf{q}_\alpha) \tag{12.3}$$

The first term is the Zeeman interaction depending upon the $\mathbf{g}(\mathbf{Q}, \mathbf{q}_\alpha)$ tensor, external magnetic field $\mathbf{B}_0$, and electron spin operator $\hat{\mathbf{S}}$; the second term is the hyperfine interaction of the nth nucleus and the unpaired electron, defined with respect to hyperfine tensor $\mathbf{A}_n(\mathbf{Q}, \mathbf{q}_\alpha)$ and nuclear spin operator $\hat{\mathbf{I}}_n$. Additional terms are $\hat{H}_{\text{probe-solvent}}(\mathbf{Q}, \mathbf{q}_\alpha)$ to account for interactions between the probe and the medium which do not affect directly the magnetic properties (e.g., solvation energy) and $\hat{H}_{\text{solvent}}(\mathbf{q}_\alpha)$ for solvent-related terms. Here tensors $\mathbf{g}$, $\mathbf{A}_h$ are diagonal in local (molecular) frames GF, A_nF; operators $\hat{\mathbf{S}}$, $\hat{\mathbf{I}}_n$ are defined in the laboratory or inertial frame (LF). An explicit dependence is left in the magnetic tensor definition from slow-probe coordinates (e.g., geometric dependence upon rotation) and solvent coordinates. The averaged density matrix becomes $\hat{\rho}(\mathbf{Q}, \mathbf{q}_\alpha, t) = \langle \hat{\rho}(\mathbf{r}_i, \mathbf{R}_k, \mathbf{q}_\alpha) \rangle_{\mathbf{r}_i, \mathbf{R}_{\text{fast}}}$ and the corresponding Liouville equation, in the hypothesis of no residual dynamic effect of averaging with respect to subpicosecond processes, can be simply written as in Eq. 12.2 with $\hat{H}(\mathbf{Q}, \mathbf{q}_\alpha)$ instead of $\hat{H}(\mathbf{r}_i, \mathbf{R}_k, \mathbf{q}_\alpha)$. The next step, that is, the projection or "elimination" of solvent/bath coordinates to obtain an effective time evolution equation depending just on the relevant set of coordinates $\mathbf{Q}$, is not a trivial passage and in truth can be addressed only in terms of a semiphenomenological, albeit very effective, theoretical approach. In essence, one assumes that averaging the density matrix with respect to solvent variables is tantamount to (1) redefining the variables as a Markov stochastic process. A simplified modified time evolution equation for $\rho(\mathbf{Q}, t)$ is defined assuming that (2) the stochastic process is not affected by the system (absence of back-reaction) and therefore that an independent equation for the conditional probability $P(\mathbf{Q}, t)$ describing the stochastic process is given by $\partial P/\partial t = -\hat{\Gamma}P$, where $\hat{\Gamma}$ is the stochastic (Fokker–Planck or Smoluchowski) operator modeling the time evolution of the reduced density matrix on relaxing processes described by stochastic coordinates $\mathbf{Q}$, with an equilibrium solution $\hat{\Gamma}P_{\text{eq}}(\mathbf{Q}) = 0$. A time evolution equation for $\rho(\mathbf{Q}, t)$ is then defined according to the so-called stochastic Liouville equation (SLE) formalism by the direct inclusion of $\hat{\Gamma}$ in the (effective) Liouville equation [2]

$$\frac{\partial \hat{\rho}}{\partial t} = -\frac{i}{\hbar}\left[\hat{H}(\mathbf{Q}), \hat{\rho}(\mathbf{Q}, t)\right] - \hat{\Gamma}\hat{\rho}(\mathbf{Q}, t) = -i\hat{\mathcal{L}}\hat{\rho} \tag{12.4}$$

where the reduced Liouvillian is defined with respect to the effective Hamiltonian

$$\hat{H}(\mathbf{Q}) = \frac{\beta_e}{\hbar}\mathbf{B}_0\mathbf{g}(\mathbf{Q})\hat{\mathbf{S}} + \gamma_e \sum_n \hat{\mathbf{I}}_n \mathbf{A}_n(\mathbf{Q})\hat{\mathbf{S}} \tag{12.5}$$

and $\mathbf{g}(\mathbf{Q})$, $\mathrm{A}_n(\mathbf{Q})$ are now averaged tensors with respect to all solvent coordinates. The inclusion of relevant variables within a phenomenological semiclassical time evolution

equation for the reduced density matrix operator of a molecular system is at the basis of the SLE, originally proposed by Kubo [36, 37] to describe the dynamics of a quantum system perturbed by a Markovian stochastic process. Formal justification of the SLE has been proposed by several authors and is reviewd by Schneider and Freed [2], and it should be clear that in the absence of a coherent theory of stochastic quantum systems, it remains a phenomenological ansatz (but see, e.g., Wassam and Freed [38, 39]). A comprehensive review of recent theoretical development of the SLE formalism is given, for instance, by Tanimura [40]. Here we point out that this is a general scheme which allows for additional considerations and further approximations. First, the average with respect to picosecond dynamic processes is carried out, in practice, together with averaging with respect to solvent coordinates to allow the QM evaluation of magnetic tensors corrected for solvent effects. Second, time separation techniques can also be applied to treat approximately relatively faster relaxing coordinates included in the relevant set $\mathbf{Q}$, such as restricted (local) torsional motions. Third, complex solvent environments (e.g., highly viscous fluids) can be described by an augmented set of stochastic coordinates, to be included in $\mathbf{Q}$, which describes slow-relaxing local solvent structures, or in other words to maintain the generalized Markovian nature of $\mathbf{Q}$.

12.2.2 Setting Up the SLE

From the spin Hamiltonian it is clear that a number of parameters are required, that is, the $\boldsymbol{g}$ tensors of the unpaired electron and the $\boldsymbol{A}$ hyperfine coupling tensors for all nuclei. All these quantities are purely quantum mechanical properties and their evaluation can be carried out via a first-principles treatment (see below). The choice of the stochastic operator, $\hat{\Gamma}$, is a basic step in the methodology. Here we comment on two canonical cases frequently occurring in standard applications: (i) rigid-body model, where the probe is seen as a rigid rotator diffusing and the stochastic variables are $\mathbf{Q} = \Omega$, the set of Euler angles which give the relative orientation of the molecule with respect to the inertial laboratory frame; (ii) "flexible"-body model, where the molecule is described as a rotator with one internal degree of freedom represented by a torsional angle, so the stochastic variables, $\mathbf{Q} = (\Omega, \theta)$, are the set of angles Ω (for the global rotation) and the torsional angle θ. In both models the stochastic variables are considered as diffusive processes and the stochastic operator has the general form

$$\hat{\Gamma} = -\hat{\nabla}_{\mathrm{Q}}^{\mathrm{tr}} \boldsymbol{D}(\mathbf{Q}) P_{\mathrm{eq}}(\mathbf{Q}) \hat{\nabla}_{\mathrm{Q}} P_{\mathrm{eq}}^{-1}(\mathbf{Q}) \tag{12.6}$$

where $\hat{\nabla}_{\mathrm{Q}}$ is the vector operator of partial derivatives over the stochastic variables, $\boldsymbol{D}(\mathbf{Q})$ is the diffusion tensor of the system (which in general may depend on the stochastic variables), and $P_{\mathrm{eq}}(\boldsymbol{Q})$ is the Boltzmann equilibrium distribution probability

$$P_{\mathrm{eq}}(\mathbf{Q}) = \frac{\exp[-V(\mathbf{Q})/kT]}{\langle \exp[-V(\mathbf{Q}) - kT] \rangle} \tag{12.7}$$

Here, $V(\boldsymbol{Q})$ is the potential acting on the stochastic coordinates and $\langle \cdot \rangle$ represents the integration over $\mathbf{Q}$. Assumptions can be made by requiring that the potential has separated contributions, for example, an "external" term acting on the global orientation (e.g., ordering effects in liquid crystals) and an internal term acting on the torsional angle (if present) which is the torsional potential, that is,

$$V(\mathbf{Q}) = V_{\text{ext}}(\Omega) + V_{\text{int}}(\theta) + V_{\text{coupling}}(\mathbf{Q}) \approx V_{\text{ext}}(\Omega) + V_{\text{int}}(\theta) \tag{12.8}$$

Mesoscopic parameters, such as the full-diffusion tensor and potential V, are usually determined phenomenologically or from complementary approaches. For instance, dissipative properties described by the diffusion tensor can be obtained on the basis of hydrodynamic modeling (see below). The internal potential can be evaluated as a potential energy surface scan over the torsional angle θ. For small molecules this operation can be easily conducted at the DFT level, while for big molecules such as proteins, mixed quantum mechanical/molecular mechanics (QM/MM) methodologies can be employed.

12.2.3 Magnetic Tensors

The introduction of the DFT is a turning point for the calculations of the spin Hamiltonian parameters [41–44]. Before DFT, ab initio calculations of the magnetic parameters of spin Hamiltonians were either prohibitively expensive already even for medium-size radicals [45–47] or less reliable than semiempirical methods. These latter were based on the approaches introduced by McConnell [48, 49] and Stone [50] for the calculations of the hyperfine coupling and the $\boldsymbol{g}$ tensors, respectively. Based on semiempirical parameters taking into account separately the spin density on the singly occupied molecular orbital (SOMO) and that due to spin polarization [51], the method for the evaluation of hyperfine tensors has been an invaluable tool for understanding the correlation between the magnetic parameters of the spin Hamiltonian, the spin distribution, the conformation of radicals, and the molecular properties in general. However, the reliability of the method was very restricted, as being limited to predictions within groups of similar radicals for which the same set of semiempirical parameters were sound, and the parameters to be calculated were only the SOMO spin densities [51]. Within these limits the calculated hyperfine tensors were quite reliable. On the other hand, the agreement between calculated and experimental values for $\boldsymbol{g}$ tensors were in general much worse. To this end, it should be noted that the recently improved methods of calculating reliable $\boldsymbol{g}$ tensors by DFT on the one hand [52–55] and to measure them by high-frequency ESR on the other has provided a new largely unexplored source of information on the molecular properties attainable by ESR analysis.

Today, the agreement between experimental and calculated parameters of the spin Hamiltonian by DFT is outstanding [41–44, 52, 56]. Both the vibrational averaging of the parameters [57–59] and the interactions of the probe with the environment [60–65] are taken into account, thus providing a set of tailored parameters that can be used confidently for further calculations. It should be noted that this approach is a step

forward with respect to the traditional starting point, that is, the use of a set of experimental hyperfine and $\boldsymbol{g}$ tensors generally obtained for a different system and extrapolated to the case of interest.

The $\boldsymbol{g}$ tensor can be dissected into three main contributions [52–56],

$$\boldsymbol{g} = g_e \mathbf{1}_3 + \Delta \boldsymbol{g}^{\mathrm{RMC}} + \Delta \boldsymbol{g}^{\mathrm{GC}} + \Delta \boldsymbol{g}^{\mathrm{OZ/SOC}} \tag{12.9}$$

where g_e is the free-electron value ($g_e = 2.002319$) and $\mathbf{1}_3$ is the 3 unit matrix; Δg^{RMC} and Δg^{GC} are first-order contributions which take into account relativistic mass (RMC) and gauge (GC) corrections, respectively. The last term, $\Delta g^{\mathrm{OZ/SOC}}$, is a second-order contribution arising from the coupling of the orbital Zeeman (OZ) and the spin–orbit coupling (SOC) operators. The SOC term is a true two-electron operator, but here it will be approximated by a one-electron operator involving adjusted effective nuclear charges [66]. This approximation has been proven to work fairly well in the case of light atoms providing results close to those obtained using more refined expressions for the SOC operator [52–54]. In our general procedure, spin-unrestricted calculations provide the zero-order Kohn–Sham (KS) orbitals and the magnetic field dependence is taken into account using the coupled-perturbed KS formalism described by Neese but including the gauge including/invariant atomic orbital (GIAO) approach [52–54]. Solution of the coupled-perturbed KS equation (CP-KS) leads to the determination of the OZ/SOC contribution.

The second term is the hyperfine interaction contribution, which in turn contains the so-called Fermi contact interaction (an isotropic term), is related to the spin density at the corresponding nucleus n by [67]

$$A_{n,0} = \frac{8\pi}{3}\frac{g_e}{g_0} g_n \beta_n \sum_{\mu,\nu} P_{\mu,\nu}^{\alpha-\beta} \langle \varphi_\mu | \delta(r_{kn}) | \varphi_\nu \rangle \tag{12.10}$$

and an anisotropic contribution which can be derived from the classical expression of interacting dipoles [68],

$$A_{n,ij} = \frac{g_e}{g_0} g_n \beta_n \sum_{\mu,\nu} P_{\mu,\nu}^{\alpha-\beta} \langle \varphi_\mu | r_{kn}^{-5} (r_{kn}^2 \delta_{ij} - 3 r_{kn,i} r_{kn,j}) | \varphi_\nu \rangle \tag{12.11}$$

The $\boldsymbol{A}$ tensor components are usually given in gauss (1 G = 0.1 mT); to convert data to megahertz one has to multiply by 2.8025.

Magnetic tensors evaluated at this level do not give sufficiently accurate estimates of experimental values, especially if one considers a molecule in a solvent with high polarity and/or a solvent that can form hydrogen bonds. Environmental effects (e.g., solvent) need to be taken into account and the most promising general approach to the problem can be based on a system–bath decomposition. Calculations can be performed on the system, including the part of the solute where the essential part of the process to be investigated is localized together with, possibly, the few solvent molecules strongly and specifically interacting with it. This part is treated at the electronic level of resolution and is immersed in a polarizable continuum, mimicking

the macroscopic properties of the solvent. So, the solution process can then be dissected into the creation of a cavity in the solute process requiring an energy E_{cav}, and the successive switching on of dispersion/repulsion, with energy $E_{dis\text{-}rep}$, and electrostatic, with energy E_{el}, interactions with surrounding solvent molecules. All of these contributionsm, for both isotropic and anisotropic solutions, are included into the so-called polarizable continuum model (PCM) [69–72]. Taking into account solvent effects gives the corrections required in order to predict values of the tensors very close to the experimental ones (see Tables 2 and 7 of ref. 73).

While in some cases considering the environment is sufficient to reproduce experimental values of the $\boldsymbol{g}$ and hyperfine tensors, there are molecules presenting fast motions in the neighborhood of the unpaired electron. Dependence of the magnetic parameters on these small geometric variations can be very significant [57, 74–76]. These motions are usually too fast with respect to the ESR time scale window so the effective contribution is a correction that can be calculated as an average over short-time dynamics calculated at a QM level [77, 78].

12.2.4 Friction and Diffusion Tensors

We review in this section a coarse-grained (hydrodynamic-based) recipe for evaluation of friction and diffusion tensors of flexible molecular systems. Let us consider a molecule made of N_A atoms which has been partitioned into N_P fragments. The ith fragment is composed of N_i atoms and its orientation relative to the $(i+1)$ th fragment is defined by the torsional angle θ_i. We limit our discussion to noncyclic molecules, so that a generic molecular system is considered in general as a sequence of N_F fragments, and the total number of torsional angles is $N_T = N_F - 1$. Notice that $\sum_{i=1}^{N_F} N_t = N_A$.

We define a molecular frame (MF) fixed on a chosen fragment v (hereafter referred to as the *main fragment*) which is placed for convenience in the center of mass of the main fragment itself (see Figures 12.1 and 12.2). The atoms in the main fragment are characterized by translational and rotational motions, while atoms belonging to the other fragments have also additional internal motions. We define the set of generalized coordinates $\boldsymbol{\mathcal{R}} = [\boldsymbol{r}, \Omega, \dot{\boldsymbol{\theta}}]$ for describing the translational and rotational coordinates of the main fragment and internal torsional motions. Associated with $\boldsymbol{\mathcal{R}}$ is the set of velocities $\boldsymbol{\mathcal{V}} = [\boldsymbol{v}, \boldsymbol{\omega}, \dot{\boldsymbol{\theta}}]$ (where the dot stands for time derivative) and also the total force consists of three contributions $\boldsymbol{\mathcal{F}} = [\boldsymbol{f}, \boldsymbol{\tau}, \boldsymbol{\tau}_i]$ corresponding, respectively, to the translational force and the global torque and internal torque moments. Forces and velocities are related by the friction tensor $\boldsymbol{\xi}$, which is defined as a $(6 + N_T) \times (6 + N_T)$ matrix

$$\begin{pmatrix} \boldsymbol{f} \\ \boldsymbol{\tau} \\ \boldsymbol{\tau}_i \end{pmatrix} = -\boldsymbol{\xi} \begin{pmatrix} \boldsymbol{v} \\ \boldsymbol{\omega} \\ \dot{\boldsymbol{\theta}} \end{pmatrix} \tag{12.12}$$

or simply $\boldsymbol{\mathcal{F}} = -\boldsymbol{\xi}\boldsymbol{\mathcal{V}}$. If one considers the system without constraints (bonds), that is, the position of each atom is independent of the positions of the other atoms, the friction tensor Ξ, of the N_A independent atoms is represented as a $3N_A \times 3N_A$ matrix.

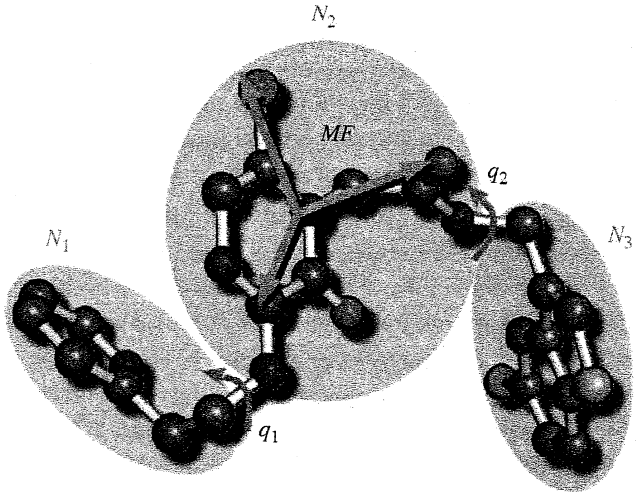

Figure 12.1 Partitioning of generic molecule into linear chain of three fragments and two torsional angles; MF is set on second fragment.

If $\boldsymbol{F}_i$ and $\boldsymbol{V}_i$ are, respectively, the translational force and velocity of the ith atom, we can write

$$\begin{pmatrix} \boldsymbol{F}_1 \\ \vdots \\ \boldsymbol{F}_{N_A} \end{pmatrix} = -\Xi \begin{pmatrix} \boldsymbol{V}_1 \\ \vdots \\ \boldsymbol{V}_{N_A} \end{pmatrix} \tag{12.13}$$

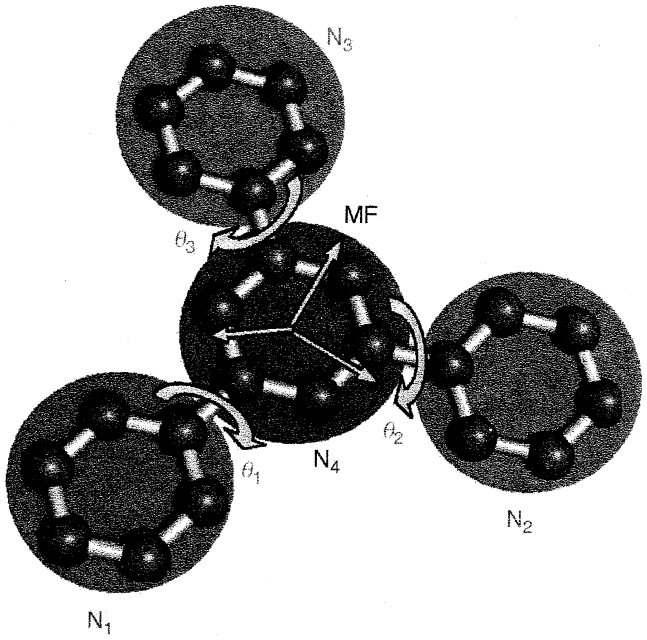

Figure 12.2 Partitioning of generic molecule in branched chain of four fragments and three torsional angles; MF is set on central fragment.

or $\boldsymbol{F} = -\Xi \boldsymbol{V}$. Following standard geometric arguments [79], one can show that $\mathcal{F} = \boldsymbol{AF}$ and $\boldsymbol{V} = \boldsymbol{B}\mathcal{V}$, where $\boldsymbol{A}$ and $\boldsymbol{B}$ are $(6 + N_T) \times 3N_A$ and $3N_A \times (6 + N_T)$ matrices which depend on the molecular geometry; additionally, $\boldsymbol{B} = A^{\text{tr}}$. It follows that

$$\xi = \boldsymbol{B}^{\text{tr}} \Xi \boldsymbol{B} = \begin{pmatrix} \xi_{TT} & \xi_{TR} & \xi_{TI} \\ \xi_{RT} & \xi_{RR} & \xi_{RI} \\ \xi_{IT} & \xi_{IR} & \xi_{II} \end{pmatrix} \tag{12.14}$$

where the subscripts stand for T = translational, R = rotational, and I = internal. The diffusion tensor is obtained from Einstein relation as the inverse of ξ,

$$\boldsymbol{D} = k_B T \xi^{-1} = \begin{pmatrix} \boldsymbol{D}_{TT} & \boldsymbol{D}_{TR} & \boldsymbol{D}_{TI} \\ \boldsymbol{D}_{RT} & \boldsymbol{D}_{RR} & \boldsymbol{D}_{RI} \\ \boldsymbol{D}_{IT} & \boldsymbol{D}_{IR} & \boldsymbol{D}_{II} \end{pmatrix} \tag{12.15}$$

where k_B is the Boltzmann constant and T the absolute temperature. The friction tensors are linked to the diffusion tensors $\boldsymbol{D}$ (constrained spheres) and $\boldsymbol{d}$ (unconstrained spheres) via the generalized Einstein relations $\boldsymbol{D} = k_B T \xi^{-1}$ and $d = k_B T\ \Xi^{-1}$. It follows that the molecular diffusion tensor for the joint translation, rotation, and internal conformational motion for the molecule, that is, D, is obtained as

$$\boldsymbol{D} = \left(\boldsymbol{B}^{\text{tr}} \boldsymbol{d}^{-1} \boldsymbol{B}\right)^{-1} \tag{12.16}$$

The main ingredients for the calculation of the diffusion tensor are the geometric matrix $\boldsymbol{B}$ and the unconstrained diffusion tensor d. Let us first consider the calculation of the geometric matrix. We define r_j^i as the vector of the ith atom in the jth fragment, u_n as the unitary vector defining the rotation θ_n, taken to be parallel to the nth torsional angle and pointing away from the main fragment, and $r_{j,k}^i$ the distance vector between the jth atom of the ith fragment and the atom at the origin of the unitary vector u_k. Atoms in the main fragment are characterized only by the translational and global rotational velocity

$$v_j^v = v + \omega \times r_j^v \tag{12.17}$$

while for the remaining fragments ($i \neq v$) the torsional contributions must be included,

$$v_j^i = v + \omega \times r_j^i + \sum_k \dot{\theta}_k u_k \times r_{j,k}^i \tag{12.18}$$

where the summation is taken over the angles that link the main fragment to the ith fragment. Equations 12.17 and 12.18 can be rewritten in matrix form as

$$v_{ij}^i = {}^T\boldsymbol{B}^i v + {}^R\boldsymbol{B}_j^i \omega + \sum_k {}^I\boldsymbol{B}_{j,k}^i \dot{\theta}_k \tag{12.19}$$

where ${}^{T}\boldsymbol{B}_j^i = 1_3$, ${}^{R}\boldsymbol{B}_j^i = \boldsymbol{r}_j^{i\times}$, and ${}^{I}\boldsymbol{B}_{j,k}^i = \boldsymbol{r}_{j,k}^{i\times}\boldsymbol{u}_k$ or 0 depending on k and i and $r_{\alpha\beta}^{\times} = r_k\xi_{\alpha\beta\gamma}$, where $\xi_{\alpha\beta\gamma}$ is the Levi-Civita tensor with $\alpha, \beta, \gamma = 1,2,3$. For a linear chain of fragments, numbered sequentially from the first to the last one, the general form of the $\boldsymbol{B}$ matrix is

$$B = \begin{pmatrix}
1_3 & \boldsymbol{r}_j^{1\times} & \boldsymbol{r}_{j,1}^{1\times}\boldsymbol{u}_1 & \cdots & \boldsymbol{r}_{j,\nu-1}^{1\times}\boldsymbol{u}_{\nu-1} & 0 & 0 & \cdots & 0 \\
1_3 & \boldsymbol{r}_j^{2\times} & 0 & \cdots & \boldsymbol{r}_{j,\nu-1}^{2\times}\boldsymbol{u}_{\nu-1} & 0 & 0 & \cdots & 0 \\
\vdots & \vdots & \vdots & \vdots & \vdots & \vdots & \vdots & \vdots & \vdots \\
1_3 & \boldsymbol{r}_j^{\nu-1\times} & 0 & \cdots & \boldsymbol{r}_{j,\nu-1}^{\nu-1\times}\boldsymbol{u}_{\nu-1} & 0 & 0 & \cdots & 0 \\
1_3 & \boldsymbol{r}_j^{\nu\times} & 0 & \cdots & 0 & 0 & 0 & \cdots & 0 \\
1_3 & \boldsymbol{r}_j^{\nu+1\times} & 0 & \cdots & 0 & \boldsymbol{r}_{j,\nu}^{\nu+1\times}\boldsymbol{u}_\nu & 0 & \cdots & 0 \\
\vdots & \vdots & \vdots & \vdots & \vdots & \vdots & \vdots & \vdots & \vdots \\
1_3 & \boldsymbol{r}_j^{N_F-1\times} & 0 & \cdots & 0 & \boldsymbol{r}_{j,\nu}^{N_F-1\times}\boldsymbol{u}_\nu & \boldsymbol{r}_{j,\nu+1}^{N_F-1\times}\boldsymbol{u}_{\nu+1} & \cdots & 0 \\
1_3 & \boldsymbol{r}_j^{N_F\times} & 0 & \cdots & 0 & \boldsymbol{r}_{j,\nu}^{N_F\times}\boldsymbol{u}_\nu & \boldsymbol{r}_{j,\nu+1}^{N_F\times}\boldsymbol{u}_{\nu+1} & \cdots & \boldsymbol{r}_{j,N_F-1}^{N_F\times}\boldsymbol{u}_{N_F-1}
\end{pmatrix} \tag{12.20}$$

The form of the geometric matrix $\boldsymbol{B}$ is dependent on the topology and also on the numbering scheme chosen for the fragments.

Evaluation of $\boldsymbol{d}$ can be carried out at the simplest possible level assuming the model of noninteracting spheres in a fluid, or one can include hydrodynamic interactions, for example, based on the Rotne–Prager (RP) approach [80, 81], which ensures a satisfactory albeit not too cumbersome treatment of sphere–sphere hydrodynamic interactions. The resulting elements of $\boldsymbol{D}$ depend upon a purely geometric tensorial component $\overline{\boldsymbol{D}}$ and the translational diffusion coefficient for an isolated sphere D_0, that is,

$$\boldsymbol{D} = D_0\overline{\boldsymbol{D}} \tag{12.21}$$

where $D_0 = k_BT/CR_e\eta\pi = k_BT/\Xi_0$: here C is a constant depending upon hydrodynamic boundary conditions, R_e is the average radius for the spheres, and η is the local viscosity. The RP unconstrained diffusion tensor is given as

$$d_{ii} = \frac{k_BT}{\Xi_0}1_3$$

$$= \begin{cases} \dfrac{k_BT}{\Xi_0}\dfrac{3R_e}{4r_{ij}^3}\left[\left(r_{ij}^2 + \dfrac{2}{3}R_e^2\right)1_3 + \left(1 - 2\dfrac{R_e^2}{r_{ij}^2}\right)r_{ij}\otimes r_{ij}\right] & \text{if } r_{ij} > 2R_e \\ \dfrac{k_BT}{\Xi_0}\left[\left(1 - \dfrac{9}{32}\dfrac{r_{ij}}{R_e}\right)1_3 + \dfrac{3}{32}\dfrac{r_{ij}\otimes r_{ij}}{r_{ij}^2}\right] & \text{if } r_{ij} < 2R_e \end{cases} \tag{12.22}$$

where i and j are two generic atoms, $\boldsymbol{r}_{ij} = \boldsymbol{r}_i - \boldsymbol{r}_j$, and $\otimes$ indicates the dyadic product. Notice that the general methodology reported above can be applied with minor changes to other types of internal motions, such as stretching of bonds, bending of bond angles, domain and loop motions.

12.2.5 Solving the SLE

Once magnetic, structural, and dissipative parameters have been estimated, the SLE is completely defined. At this point, physical properties can be calculated, with the knowledge of $\hat{\Gamma}$ and P_{eq}, either directly from the conditional probability $P(\boldsymbol{X}, t)$ or in terms of time correlation functions, which are defined, for two correlated observables $f(\mathbf{Q}, t)$ and $g(\mathbf{Q}, t)$, as

$$G(t) = \langle f(\mathbf{Q}, t) | \exp(-\hat{\Gamma} t) | g(\mathbf{Q}, t) P_{eq}(\mathbf{Q}) \rangle \tag{12.23}$$

from which it is possible to calculate the spectral density, that is, the Fourier–Laplace transform of G(t), as

$$J(\omega) = \frac{1}{\pi} \int_0^\infty d\omega \, G(t) e^{-i\omega t} = \frac{1}{\pi} \langle f(Q, t) | (i\omega + \hat{\Gamma})^{-1} | g(\mathbf{Q}, t) P_{eq}(\mathbf{Q}) \rangle \tag{12.24}$$

The formalism for evaluating cw-ESR spectra is now easily interpreted in terms of spectral densities. In the SLE framework, the stochastic operator $\hat{\Gamma}$ is part of the generic stochastic Liouvillian $\hat{\mathcal{L}}$ and the cw-ESR spectrum is given by

$$I(\omega - \omega_0) = \frac{1}{\pi} \mathcal{R}e \left\{ \left\langle \left\langle \upsilon \left| \left[i(\omega - \omega_0) + \hat{\mathcal{L}} \right]^{-1} \right| \upsilon P_{eq} \right\rangle \right\rangle \right\} \tag{12.25}$$

that is, as the real part of the spectral density for the autocorrelation function for the observable, usually called the *starting vector*, corresponding to the X component of the magnetization as well as P_{eq}.

It is convenient to transform the Liouvillian with the symmetrization

$$\tilde{\mathcal{L}} = P_{eq}^{-1/2} \hat{\mathcal{L}} P_{eq}^{1/2} = i\hat{\mathcal{H}}^\times + P_{eq}^{-1/2} \hat{\Gamma} P_{eq}^{1/2} = i\hat{\mathcal{H}}^\times + \tilde{\Gamma} \tag{12.26}$$

where the density matrix is $\tilde{\rho}(\boldsymbol{Q}, t) = \rho(\boldsymbol{Q}, t) / \rho_{eq}(\boldsymbol{Q})$ and the equilibrium probability density is $\tilde{P}_{eq} = P_{eq}^{1/2}$. The spectral density becomes

$$I(\omega - \omega_0) = \frac{1}{\pi} \mathcal{R}e \left\{ \left\langle \left\langle \upsilon P_{eq}^{1/2} \left| \left[i(\omega - \omega_0) + i\hat{\mathcal{H}}^\times + \tilde{\Gamma} \right]^{-1} \right| \upsilon P_{eq}^{1/2} \right\rangle \right\rangle \right\} \tag{12.27}$$

The definition of the starting vector depends on the radical studied. Consider as an example the case of a monoradical in which the unpaired electron is coupled to a nucleus of spin I: The starting vector takes the form

$$\left| \upsilon P_{eq}^{1/2} \right\rangle \rangle = (2I + 1)^{-1/2} \left| \hat{S}_X \times 1_I \times P_{eq}^{1/2} \right\rangle \rangle \tag{12.28}$$

The cw-ESR spectrum is obtained by numerically evaluating the spectral density defined in Eq. 12.27, and here we adopt the standard methodology of spanning the Liouvillian over a proper basis set defined by the direct product

$$\left|\sum\right\rangle\!\rangle = \left|\sigma\right\rangle\!\rangle \otimes \left|\Lambda\right\rangle \tag{12.29}$$

The basis set for the spin coordinates, $|\sigma\rangle\!\rangle$ is the space of spin transitions and is defined elsewhere [2, 9, 82]. For the stochastic part we make the standard choice of employing Wigner rotation matrices for the global rotation and complex exponentials for the internal torsional angle, that is, $|\Lambda\rangle = |LMK\rangle \otimes |n\rangle$ with,

$$|LMK\rangle = \sqrt{\frac{2L+1}{8\pi^2}} D^L_{Mk}(\Omega) \tag{12.30}$$

$$|n\rangle = \frac{1}{\sqrt{2\pi}} e^{-in\theta} \tag{12.31}$$

To obtain the spectral density, usually iterative algorithms such as Lanczos [83, 84] or conjugate gradients [2] are employed. In particular, we make use of the Lanczos algorithm, a recursive procedure to generate orthonormal functions which allow a tridiagonal matrix representation of the system Liouvillian. Assuming as a first function the normalized zero-average observable, $|1\rangle\!\rangle = |\upsilon P_{\text{eq}}^{1/2}\rangle\!\rangle / \langle\!\langle \upsilon | P_{\text{eq}} | \upsilon \rangle\!\rangle 1/2$, the following functions are obtained recursively:

$$\beta_{n+1}|n+1\rangle\!\rangle = (\tilde{\mathcal{L}} - \alpha_n)|n\rangle\!\rangle - \beta_n |n-1\rangle\!\rangle \tag{12.32}$$

$$\alpha_n = \langle\!\langle n|\tilde{\mathcal{L}}|n\rangle\!\rangle \tag{12.33}$$

$$\beta_n = \langle\!\langle n|\tilde{\mathcal{L}}|n-1\rangle\!\rangle \tag{12.34}$$

Coefficients α_n and β_n actually form the first and second diagonal of the tridiagonal (complex) symmetric matrix representation of the symmetrized Liouvillian, and the spectrum can be written in the form of a continued fraction [84]

$$I(\omega) = \cfrac{1}{i\omega - \alpha_1 - \cfrac{\beta_2^2}{i\omega - \alpha_2 - \cfrac{\beta_3^2}{i\omega - \alpha_3 - \cdots}}} \tag{12.35}$$

Evaluation of Eqs. 12.32–12.34 is carried on in finite arithmetic by projecting the symmetrized Liouvillian and the starting vector on the basis set 12.29, defining the matrix operator and starting vector elements

$$\mathcal{L} = \left\langle\!\left\langle \sum \middle| \tilde{\mathcal{L}} \middle| \sum' \right\rangle\!\right\rangle \tag{12.36}$$

$$\upsilon = \left\langle\!\left\langle \sum \middle| 1 \right\rangle\!\right\rangle \tag{12.37}$$

so that the matrix–vector counterparts of Eqs. 12.32–12.34 become

$$\beta_{n+1}\upsilon_{n+1} = (\mathcal{L} - \alpha_n)\upsilon_n - \beta_n\upsilon_{n-1} \tag{12.38}$$

$$\alpha_n = \upsilon_n \cdot \mathcal{L} \cdot \upsilon_n \tag{12.39}$$

$$\beta_n = \upsilon_n \cdot \mathcal{L} \cdot \upsilon_{n-1} \tag{12.40}$$

Symmetry arguments can be employed to significantly reduce the number of basis function sets required to achieve convergence, together with numerical selection of a reduced basis set of functions based on "pruning" of basis elements with negligible contributions to the spectrum [2]. New strategies for reducing matrix dimensions in densely coupled spin systems are being investigated [85].

12.2.6 Case Study: Interpretation of cw-ESR Spectra of Tempo-Palmitate in 5CB

In the following we perform a complete a priori simulation of the ESR spectra of the prototypical nitroxide probe 4-(hexadecanoyloxy)-2,2,6,6-tetramethylpiperidine-1-oxy (usually referred to as Tempo-palmitate, TP) in isotropic and nematic phases of 5CB, for which detailed cw-ESR data are available in the literature [86]. The system is described as a flexible body reorienting under the influence of an external field, which favors its orientation along the nematic director, which is assumed parallel to the external magnetic field along the Z axis of the inertial laboratory frame (LF). We shall adopt a number of simplifying hypotheses aimed at keeping the required computational effort at a reasonable level. The molecule is considered as split into two fragments, the alkyl chain and the paramagnetic probe (Tempo) (Figure 12.3). Geometry and dynamics are described by two stochastic variables: (i) the set of Euler angles (Ω) which describes the orientation between the LF and a molecule fixed frame (MF) and (ii) an internal angle (θ) which defines the relative orientation between the Tempo fragment and the alkyl chain.

Structural properties were obtained by means of quantum mechanical calculations performed to find the minimum energy geometry of the molecule, evaluate the magnetic tensors, and calculate the internal potential [44]. On the basis of a previous study [87], the alkyl chain of TP was replaced by an ethyl group. Internal torsional potentials and magnetic tensors were then evaluated by the PBE0 hybrid functional [88] and the purposely tailored N06 basis set. Solvent effects were taken into account by our anisotropic version of the polarizable continuum model [87].

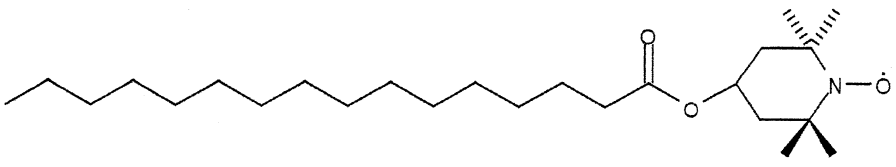

Figure 12.3 Molecular structure of Tempo-palmitate.

Of course, the diffusion tensor was evaluated for the true TP radical using the geometry optimized for the all-trans conformer.

The MF is fixed on the alkyl chain, which is considered as a rigid entity in the all-trans conformation; the MF is chosen in such a way that the rotational part of the diffusion tensor (see below) is diagonal. Magnetic tensors are diagonal in the same reference frame (μF) fixed on paramagnetic probe. The total potential energy of the system is defined according to Eq. 12.8, that is, we neglect potential coupling terms $V_{\text{coup}}(\Omega, \theta)$ between internal (θ) and external (Ω) variables (Figure 12.5). The external potential is chosen according to the simple Maier–Saupe form [89–91]

$$U_{\text{ext}} = \frac{V_{\text{ext}}}{k_B T} = -\epsilon \mathcal{D}^2_{0,0}(\Omega) \tag{12.41}$$

This is the simplest potential which assures the presence of an energy minimum when the alkyl chain is parallel to the nematic director.

An accurate evaluation of the internal deg potential is obtained directly by QM calculations. An energetic barrier is observed corresponding to $\theta = 180°$. In general, we may define the potential via the expansion $V_{\text{int}}/k_B T = -\sum \chi_n e^{-in\theta}$, where $\chi_n = \chi^*_{-n}$ ensure that the potential is real. In practice terms up to $n = 1$ have been retained to fit the potential to the shifted cosine form

$$U_{\text{int}} = \frac{V_{\text{int}}}{k_B T} \approx A(1 - \cos\theta) \tag{12.42}$$

To summarize, energetics is defined by the simplified expression

$$U = U_{\text{ext}} + U_{\text{int}} = -\epsilon \mathcal{D}^2_{0,0}(\Omega) + A(1 - \cos\theta) \tag{12.43}$$

defined by parameters ϵ and A.

In the case under investigations, which includes nematic (anisotropic) phase environments, we shall assume the usual approximation of considering isotropic local friction, and the macroscopic local viscosity is taken equal to half of the fourth Leslie–Ericksen coefficient η_4 [92–95]. The diffusion tensor of the system is obtained, neglecting translational contributions, as a 4×4 matrix, that is,

$$\boldsymbol{D} = \begin{pmatrix} \boldsymbol{D}_{RR} & \boldsymbol{D}_{RI} \\ \boldsymbol{D}_{IR} & \boldsymbol{D}_{II} \end{pmatrix} \tag{12.44}$$

where the 3×3 $\mathbf{D}_{RR}$ block is the purely rotational contribution, the $\boldsymbol{D}_{IR} = \boldsymbol{D}^{\text{tr}}_{RI}$ blocks describe the rotoconformational interaction, and $\boldsymbol{D}_{II}$ is the conformational diffusion coefficient. The general outcome of the elements of the 4×4 diffusion tensor shows, as expected, a weak dependence upon the internal angles. We express the tensor as

$$\boldsymbol{D}(T) = D(T)\bar{\boldsymbol{d}} \tag{12.45}$$

in order to separate the purely geometric tensorial component $\bar{\boldsymbol{d}}$ and the translational diffusion coefficient for an isolated sphere $D(T)$, that is, $D(T) = k_B T/CR_{\pi\eta}(T)$: Here

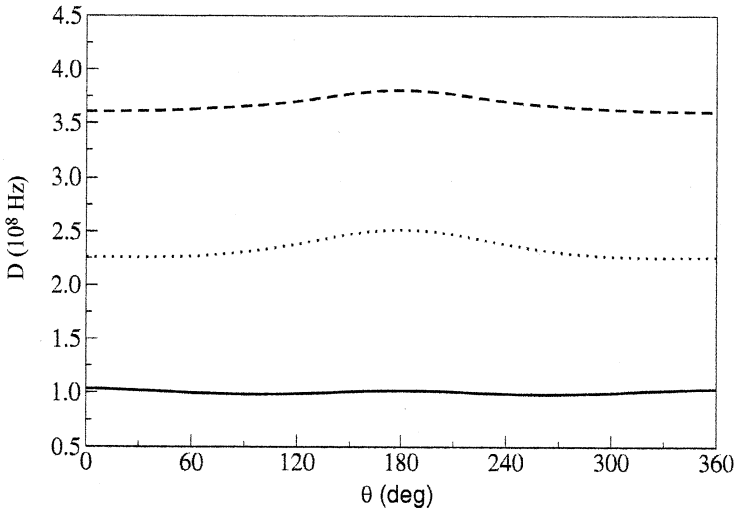

Figure 12.4 Values of $\mathrm{Tr}\boldsymbol{D}_{RR} \times 10^{-7}$ s (full line), $|D_{RI}| \times 10^{-7}$ s (dashed line), and $D_{II} \times 10^{-7}$ s (dotted line) for $T = 316.09$ K plotted vs. conformation angle θ.

C is a constant depending on hydrodynamic boundary conditions, R is the average radius for the spheres, and η is the local viscosity.

Selected tensor functions of the diffusion tensor, namely $Tr\{D_{RR}\}$, $|D_{RI}|$, and D_{II}, are shown for $T = 316.92$ K in Figure 12.4 as function of θ: Variation is indeed minimal; therefore we assume the diffusion tensor calculated for the minimum energy configuration ($\theta = 0$).

Next we need to define the form of the time evolution operator (Liouvillian) for the density matrix described by the SLE. The molecule being partitioned in two fragments, as described above, we have (i) two local frames respectively fixed on the palmitate chain (CF) and on the tempo probe (PB): these are chosen with their respective z axes directed along the rotating bond, for convenience; (ii) the molecular frame (MF), fixed on the palmitate chain: this is the frame which diagonalizes the

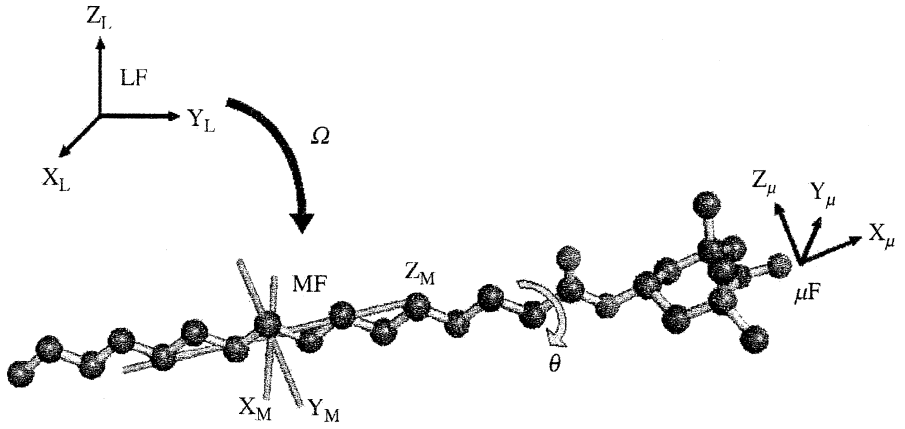

Figure 12.5 Relevant stochastic coordinates.

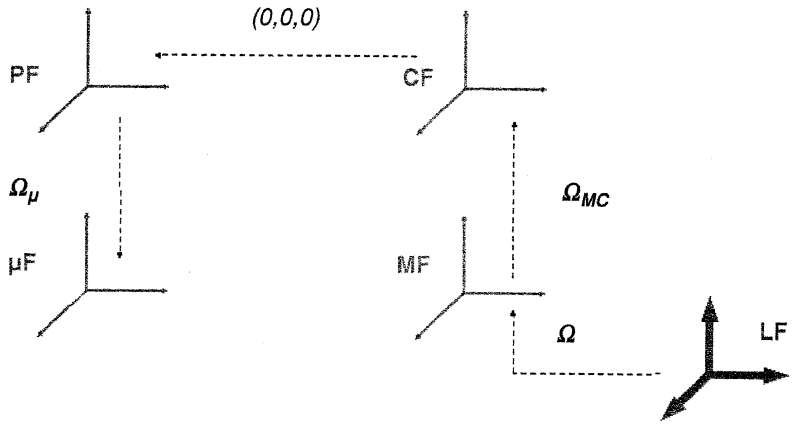

Figure 12.6 Molecular frames and Euler angle sets employed in the model.

rotational part of the diffusion tensor $\boldsymbol{D}_{RR}$; the magnetic frame, fixed on the probe (μF) where magnetic tensors are diagonal (Figure 12.6). Several sets of Euler angles are defined: Ω_{MC} is the set of Euler angles that transforms MF to CF, which has the z axis parallel to the rotating bond, Ω_μ is the set of Euler angles that transforms from PF to μF; the set (0, 0, θ) is the rotation from CF to PF; finally Ω transforms from the laboratory frame LF to MF. Following the established methodology [2, 30, 82, 84] the general form of the spin super-Hamiltonian is cast in the contracted tensorial form

$$\hat{H}^{\times} = \sum_{\mu} \omega_\mu \sum_{l=0,2} \sum_{m=-l}^{l} F^{(l,m)}_{\mu,\mathrm{LF}} * \hat{A}^{(l,m)\times}_{\mu,\mathrm{LF}} \tag{12.46}$$

where $\mu = g, A$ runs over the magnetic interactions, that is, the Zeeman interaction between the electron and the external field (g) and the hyperfine interaction between the electron and the ^{14}N nucleus (A). Parameters ω_μ, with $\mu = g, A$ are defined as $\beta_e B_0$ Tr $\boldsymbol{g}/3\hbar$ and γ_eTr $\boldsymbol{A}/3$, respectively. Notice that for the generic irreducible spherical tensor F one can write

$$F^{(l,m)}_{\mu,\mathrm{LF}} * = \sum_{m',m''} D^{l}_{m,m'}(\Omega) e^{-im''\theta} G^{(l,m',m'')}_{\mu} \tag{12.47}$$

with

$$G^{(l,m,m')}_{\mu} = \mathcal{D}^{l}_{m,m'}(\Omega_{\mathrm{MC}}) \sum_{m''} D^{l}_{m',m''}(\Omega_\mu) F^{(l,m'')}_{\mu,\mu\mathrm{F}} * \tag{12.48}$$

Explicit forms for $F^{(l,m)}_{\mu,\mu\mathrm{F}} *$ and superoperators $\hat{A}^{(l,m)\times}_{\mu,\mathrm{LF}}$ are provided in the literature [82].

Finally, we define the form of the diffusion operator. In a symmetrized form (vide supra) we write

$$\tilde{\Gamma} = -P_{\mathrm{eq}}^{1/2} \left(\frac{\hat{M}}{\partial} \frac{\partial}{\partial \theta} \right)^{\mathrm{tr}} \mathbf{D} P_{eq} \left(\frac{\hat{M}}{\partial} \frac{\partial}{\partial \theta} \right) P_{\mathrm{eq}}^{-1/2} = \tilde{\Gamma}_{RR} + \tilde{\Gamma}_{II} + \tilde{\Gamma}_{RI} \tag{12.49}$$

where $\tilde{\Gamma}$ acts on $X = (\Omega, \theta)$, the set of relevant variables; $\hat{M}$ is the infinitesimal rotation operator. Finally, for the explicit evaluation of matrix elements, it is convenient to define

$$\begin{aligned}
\tilde{\Gamma}_{RR} &= -P_{eq}^{-1/2}\hat{M}^{tr}\boldsymbol{D}_{RR}P_{eq}\hat{M}P_{eq}^{-1/2} \\
\tilde{\Gamma}_{II} &= -D_{II}P_{eq}^{-1/2}\frac{\partial}{\partial\theta}P_{eq}\frac{\partial}{\partial\theta}P_{eq}^{-1/2} \\
\tilde{\Gamma}_{RI} &= -P_{eq}^{-1/2}\left(\hat{M}^{tr}\boldsymbol{D}_{RI}P_{eq}\frac{\partial}{\partial\theta} + \frac{\partial}{\partial\theta}\boldsymbol{D}_{IR}P_{eq}\hat{M}\right)P_{eq}^{-1/2}
\end{aligned} \tag{12.50}$$

The detailed forms of the rotational, internal, and rotational–internal operators are reported elsewhere [2, 30, 82, 84]. Although rather cumbersome, the whole algebraic derivation is straightforward. The numerical solution is based on the standard methodology described above.

Let us first report on the calculated set of parameters obtained from the QM calculations for structural and magnetic properties and the hydrodynamic modeling for diffusion properties. The principal values of the magnetic tensors minus the isotropic part are $g_{xx} = 0.00221$, $g_{yy} = 0.00020$, $g_{zz} = -0.00240$, $A_{xx} = -9.19$ G, $A_{yy} = -8.98$ G, and $A_{zz} = 18.18$ G. The orientations of the internal frames of reference are specified by angles $\Omega_{MC} = (90, 35, 0)$ degrees and $\Omega_{\mu} = (0, 55, 180)$ degrees. The isotropic values of the hyperfine and gyromagnetic tensors are significantly different for different phases and are taken from experiment (see Table 12.1). A comparison with QM computed values is discussed in the next section. The computed torsional barrier of 1.8 kcal/mol^{-1} for the θ angle leads to a potential parameter $A = 453$ K/T. The diffusion tensor is expressed by Eq. 12.45 with

$$\bar{d} = \begin{pmatrix}
2.387 \times 10^{-3} & 0.0 & 0.0 & 1.560 \times 10^{-2} \\
0.0 & 2.989 \times 10^{-3} & 0.0 & 1.313 \times 10^{-2} \\
0.0 & 0.0 & 4.513 \times 10^{-2} & -3.071 \times 10^{-2} \\
1.560 \times 10^{-2} & 1.313 \times 10^{-2} & -3.071 \times 10^{-2} & 5.884 \times 10^{-2}
\end{pmatrix} \text{Å}^2 \tag{12.51}$$

Table 12.1 Parameters Employed in Simulations

T/K	A_{iso}/Gauss	g_{iso}	ϵ	η/mPa s
316.09	15.5	2.00615	0.0	18.89
309.03	15.5	2.00629	0.0	23.80
308.72	15.7	2.00659	0.0	25.78
307.88	14.7	2.00679	0.9	26.80
299.02	13.5	2.00706	1.0	31.70

and

$$D(T) = D(T_0)\frac{\eta(T_0)}{\eta(T)}\frac{T}{T_0}$$

where $D(T_0)$ is the translational diffusion coefficient for a sphere of radius R at reference temperature T_0 given by

$$D(T_0) = \frac{k_B}{RC}\frac{T_0}{\pi\eta(T_0)}$$

Choosing $R = 2.0$ Å, $C = 6$, $T_0 = 316.92$ K (as reference temperature), and, $\eta(T_0) = 18.89 \times 10^{-3}$ Pa s, one gets $D(T_0) = 6.12 \times 10^9$ Hz.

We can now simulate the cw-ESR spectra of the Tempo-palmitate in 5-cyanobiphenyl in the range of temperatures from 316.92 K (isotropic phase) to 299.02 K (nematic phase). In Figure 12.7 simulated spectra are reported superimposed on experimental spectra taken from the literature [86]. The spectra at different temperatures and in different phases are reproduced with a very limited number of fitting parameters (ordering potential and isotropic parts of the magnetic tensors).

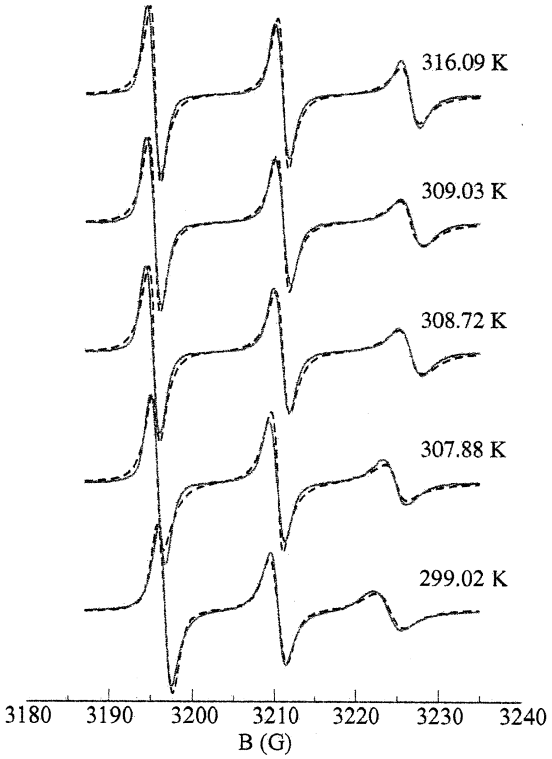

Figure 12.7 Experimental (full line) and simulated (dashed line) cw-ESR spectra of Tempo-palmitate in 5-cianobiphenyl at 316.09, 309.03 K (isotropic phase), 308.72 K (isotropic–nematic transition) and 307.88, 299.02 K (nematic phase).

12.3 INTERPRETING NMR RELAXATION DATA IN MACROMOLECULES

Spectroscopic techniques, both magnetic and optical, are widely used in structural and dynamical investigation of microscopic parameters of biomolecules [96], and, in particular, nuclear magnetic resonance (NMR) spectroscopy showed to be an important and powerful experimental technique in the interpretation of the microdynamics of proteins. The macroscopic physical observables are the T_1, T_2 and NOE relaxations of ^{15}N, ^{2}H, and ^{13}C nuclei, which have been found to be very sensitive to dynamics. The interpretative potential of the methodology comes from the fact that isotopic enrichment can be targeted to single residues of the protein, leading to the possibility of understanding localized dynamics (e.g., studying conformational motions specifically in the active site of the protein) and, moreover, comparison of data coming from different residues of the same protein permits us to make spatial (structural) considerations.

NMR relaxation data depend on dipolar (^{15}N and ^{13}C) and quadrupolar (^{2}H) interactions on chemical shift anisotropy and cross-correlation effects. It is well known that the NMR relaxations can be written as functions of the spectral densities of the magnetic interactions, and this is the intersecting point between macroscopic and microscopic descriptions: The spectral densities are calculated within the theoretical framework describing the dynamics of the system.

The most challenging part of the work is the introduction of the theoretical model. An early approach was proposed by Lipari and Szabo [97, 98] with their "model free" (MF) analysis. This approach is based on considering the presence of two uncoupled motions in the system: the global tumbling of the protein and the local motion of the probe. The assumption of decoupling leads to an easy formulation for the spectral density as the sum of spectral densities calculated from the two different motions. Simple mathematical expressions and fast calculations come from this approach, but also a number of limitations, leading to a restricted range of validity. The two most important limitations of their approach are: (i) MF considers isotropic global tumbling of the protein so that it works well with globular proteins but not with other molecules the geometry of which is not well approximated by a sphere (in later versions anisotropy was introduced); (ii) it fails to reproduce NMR data when the time scales of the motions are similar, that is, where the decoupling approximation cannot be assumed a priori.

An advanced approach to the modeling of two coupled dynamical processes was introduced by Polimeno and Freed [9, 30], originally in the interpretation of the electron spin resonance (ESR) of probes in ordered phases such as liquid cystals and glasses [8, 99]. The model is known as the slowly relaxing local structure (SRLS) model, which is a two-body Smoluchowski equation describig the coupled motion of two rigid rotors. This model has been applied by Meirovitch et al. [100–102] to the interpretation of NMR data. Due to the fact that coupled relaxation is taken into account rigorously and because the interaction potential can be interpreted in terms of local ordering imposed by the protein to the probe, the SRLS model has been shown to

be useful, yielding good fitting to experiment even in cases that are out of the range of validity of the MF approach.

12.3.1 Two-Body Stochastic Modeling

Magnetic relaxation times T_1, T_2 and NOE of ^{15}N, ^{13}C, and ^{2}H nuclei depend on dipolar (^{15}N and ^{13}C) and quadrupolar (^{2}H) interactions, chemical shift anisotropy, and cross-correlation effects. In particular, we consider here as a spin probe the $^{15}N-^{1}H$ bond for which, following standard theory [103], it is possible to express the NMR relaxation times as functions of the spectral densities $J^D(\omega)$ (dipolar interaction) and $J^C(\omega)$ (chemical shift anisotropy):

$$\begin{aligned}
\frac{1}{T_1} &= d^2[J^D(\omega_H-\omega_N)+3J^D(-\omega_N)+6J^D(\omega_H-\omega_N)]+c^2J^C(-\omega_N)\\
\frac{1}{T_2} &= d^2[4J^D(0)+J^D(\omega_H-\omega_N)+3J^D(-\omega_N)+3J^D(\omega_H)+6J^D(\omega_H-\omega_N)]\\
&\quad+\frac{1}{3}c^2[3J^C(-\omega_N)+4J^C(0)]\\
\mathrm{NOE} &= 1+d^2\frac{\gamma_H}{\gamma_N}T_1[6J^D(\omega_H+\omega_N)-J^D(\omega_H-\omega_N)]
\end{aligned} \tag{12.52}$$

where $d=\mu_0\gamma_H\lambda_N/4\pi r_{NH}^3$, $c=\sqrt{2/15}\omega_N/\delta_{CSA}$, δ_{CSA} is the anisotropy of the chemical shift tensor, and ω_A is the Larmor frequency of nucleus A.

Spectral densities are calculated within the framework of the theoretical model for the dynamical evolution of the system. In the SRLS approach a two-body Smoluchowski equation describes the time evolution of the density probability of two relaxation processes (at different time scales) coupled by an interaction potential. In the application of this model to the description of protein dynamics, the two relaxing processes are interpreted as the slow global tumbling of the whole protein and the relatively fast local motion of the spin probe, the local motion of the $^{15}N-^{1}H$ bond in our case. Both processes are described as rigid rotators the motion of which is coupled by a potential correlating their reorientation, and it is interpreted as providing the local ordering that the molecule imposes on the probe.

Figure 12.8 gives a complete overview of the relevant coordinates and frames which are invoked in the model:

LF is the fixed inertial laboratory frame.

M_1F is the protein fixed frame where the diffusion tensor of the protein, ${}^{M_1}\boldsymbol{D}$, is diagonal.

M_2F is the protein fixed frame where the diffusion tensor of the probe, ${}^{M_2}\boldsymbol{D}$, is diagonal.

VF is the protein fixed frame having the z axis aligned with the director of the orienting potential.

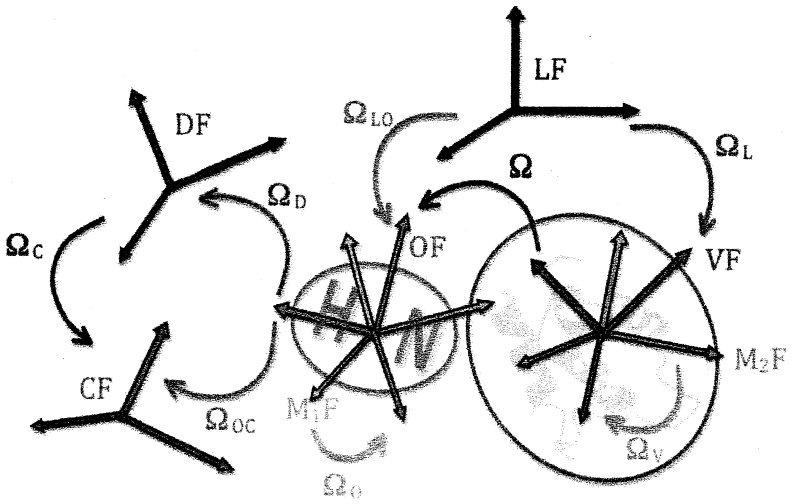

Figure 12.8 Definition of frames and Euler angles in SRLS model applied to NMR.

OF is the probe fixed frame the z axis of which tends to be aligned to the director of the potential.

DF is the probe fixed frame where the dipolar interaction is diagonal.

CF is the probe fixed frame where the chemical shift tensor is diagonal.

To complete the picture, we have to define the set of Euler angles that transform among the different frames:

Ω_L transform from LF to VF, while Ω_{LO} transform from LF to OF.

Ω tranform from VF to OF.

Ω_V tranform from M_1F to VF.

Ω_O transform from M_2F to OF.

Ω_C transform from OF to DF, while Ω_{OC} tranform from OF to DF.

Ω_C transform from CF to DF.

The system is fully described with two sets of stochastic Euler angles, and in particular our choice is on the set of Euler angles Ω_L, giving the orientation of the protein relative to the laboratory frame, and Ω, which represents the relative orientation of the probe and the protein. Using this set of stochastic variables, $\mathbf{Q} = (\Omega, \Omega_L)$, the diffusion operator describing the time evolution of the density probability of the system is

$$\hat{\Gamma}(\mathbf{Q}) = {}^{O}\hat{\mathbf{J}}^{\dagger}(\Omega)\,{}^{O}\mathbf{D}P_{\mathrm{eq}}(\mathbf{X})\,{}^{O}\hat{\mathbf{J}}(\Omega)P_{\mathrm{eq}}^{-1}(\mathbf{Q}) + \left[V\hat{\mathbf{J}}(\Omega) - {}^{V}\hat{\mathbf{J}}(\Omega_L)\right]^{\dagger V}\mathbf{D}_1 P_{\mathrm{eq}}(\mathbf{Q})\left[V\hat{\mathbf{J}}(\Omega) - {}^{V}\hat{\mathbf{J}}(\Omega_L)\right]P_{\mathrm{eq}}^{-1}(\mathbf{Q}) \qquad (12.53)$$

where ${}^{0}\mathbf{D}_2$ is the diffusion tensor of the probe in OF, ${}^{V}\mathbf{D}_1$ is the diffusion tensor of the protein in VF, and the equilibrium distribution $P_{eq}(\mathbf{X})$ is given by

$$P_{eq}(\mathbf{Q}) = \mathcal{N} \exp\left[-\frac{V(\Omega, \Omega_L)}{k_B T}\right] \tag{12.54}$$

We may assume that the protein is immersed in an isotropic medium, so the equilibrium distribution is independent of Ω_L and the total potential is just the interaction potential between the two processes for which we take the following expansion over Wigner matrices:

$$-\frac{V(\Omega)}{kT} = c_0^2 \mathcal{D}^2_{0\,0}(\Omega) + c_2^2[\mathcal{D}^2_{0\,-2}(\Omega) + \mathcal{D}^2_{0\,2}(\Omega)] + c_0^4 \mathcal{D}^4_{0\,0}(\Omega) + c_2^4[\mathcal{D}^4_{0\,-2}(\Omega) + \mathcal{D}^4_{0\,2}(\Omega)] + c_4^4[\mathcal{D}^4_{0\,-4}(\Omega) + \mathcal{D}^4_{0\,4}(\Omega)] \tag{12.55}$$

Observables are expressed as spectral densities, that is, Fourier–Laplace transforms of correlation functions of Wigner functions of the absolute probe Euler angles, $\Omega_{LO} = \Omega + \Omega_L$

$$j_{k,k'}(\omega) = \langle \mathcal{D}^j_{mk}(\Omega_{LO}) P_{eq}(\Omega_{LO}) | (i\omega - \hat{\Gamma})^{-1} | \mathcal{D}^{j'}_{m'k'}(\Omega_{LO}) P_{eq}(\Omega_{LO}) \rangle \tag{12.56}$$

Considering the symmetry of the magnetic interactions (dipolar and chemical shift anisotropy) contributing to the spin Hamiltonian of the system for the ^{15}N–^{1}H probe, only physical observables with $j = j' = 2$ and $m = m' = 0$ have to be considered.

From these spectral densities it is possible to calculate the spectral densities for every magnetic interaction, μ (dipolar, CSA), as

$$J^{\mu}(\omega) = \sum_{k,k'=-2}^{2} [\mathcal{D}^{2\,*}_{k\,0}(\Omega_\mu) \mathcal{D}^2_{k'0}(\Omega_\mu)]\, jk, k'(\omega) \tag{12.57}$$

where Ω_μ is the set of Euler of angles transforming from OF to the frame where the μth magnetic tensor is diagonal.

Calculation of spectral densities $j_{k,k'}(\omega)$ is achieved by spanning the diffusive operator over a proper basis set, as usual. An obvious choice is the direct product $|\Lambda\rangle = |\lambda_1\rangle \otimes |\lambda_2\rangle = |L_1 M_1 K_1\rangle \otimes |L_2 M_2 K_2\rangle$, where

$$|L_1 M_1 K_1\rangle = \sqrt{\frac{2L_1 + 1}{8\pi^2}} \mathcal{D}^{L_1}_{M_1 K_1}(\Omega_L) \tag{12.58}$$

$$|L_2 M_2 K_2\rangle = \sqrt{\frac{2L_2 + 1}{8\pi^2}} \mathcal{D}^{L_2}_{M_2 K_2}(\Omega) \tag{12.59}$$

It is simpler to work with autocorrelation functions so instead of directly calculating spectral densities in Eq. 12.56, we define the function $2C_{k,k'} = \mathcal{D}^2_{0k} + \mathcal{D}^2_{0k'}$, and calculate the symmetrized spectral densities

$$j^S_{k,k'}(\omega) = \langle C_{k,k'}(\Omega_{LO}) P_{\mathrm{eq}}(\Omega_{LO}) \big| \big(i\omega - \hat{\Gamma}\big)^{-1} \big| C_{k,k'}(\Omega_{LO}) P_{\mathrm{eq}}(\Omega_{LO}) \rangle \tag{12.60}$$

and then obtain the $j_{k,k'}(\omega)$ functions as linear combinations of the symmetrized spectral densities:

$$j_{k,k'}(\omega) = \frac{1}{10}\left[2(1+\delta_{k,k'}) j^S_{k,k'}(\omega) - j^S_{k,k}(\omega) - j^S_{k',k'}(\omega)\right] \tag{12.61}$$

Using the closure relation for the basis $|\Lambda\rangle$, the integral in Eq. 12.60 can now be rewritten in matrix form as

$$j^S_{k,k'} = \boldsymbol{v}^t (i\omega 1 - \Gamma)^{-1} \boldsymbol{v} \tag{12.62}$$

where

$$(\Gamma)_{i,j} = \langle \Lambda_i | \hat{\Gamma} | \Lambda_j \rangle \tag{12.63}$$

$$(\boldsymbol{v})_i = \langle \Lambda_i | C_{k,k'}(\Omega_{LO}) P_{\mathrm{eq}}(\Omega_{LO}) \rangle \tag{12.64}$$

Details on the evaluation of eqs. 12.63 and 12.64 are reported elsewhere [100].

12.3.2 Case Study: AKeko Protein

A set of residues of the *Escherichia coli* adenylate kinase (AKeco) protein has been selected in order to illustrate and test the application of the methodology to real experimental data. In Figure 12.9 are highlighted the chosen residues with different colors. The color scheme is: yellow for the AMPbd domain, red for the CORE domain, blue for the LID domain, and green for the small P-loop. We followed the standard definition in dividing the protein into those domains [100]. For the experimental values see the supporting information in Shapiro et al. [100].

The diffusion tensor of the protein, in water, was evaluated with slip boundary conditions, effective radius of the spheres of 2.0 Å, and room temperature and viscosity of 0.9 cP. With this parameters we obtained ${}^1D_{XX} = 1.11 \times 10^7$ Hz, ${}^1D_{YY} = 1.20 \times 10^7$ Hz, and ${}^1D_{ZZ} = 1.65 \times 10^7$ Hz. Because of the near axiality of the tensor, in the calculations we assumed the average values ${}^1D_{XX} = {}^1D_{YY} = 1.15 \times 10^7$ Hz. We imposed an axial orienting potential coupling the two bodies.

As outlined above, the first body describes the motion of the protein, while we interpret the second body as the (collective) local motions in the neighborhood of the magnetic probe, the ^{15}N–^{1}H bond. In this picture we assume, for the second body, a diffusion tensor which is diagonal in a frame having the Z axis parallel to the

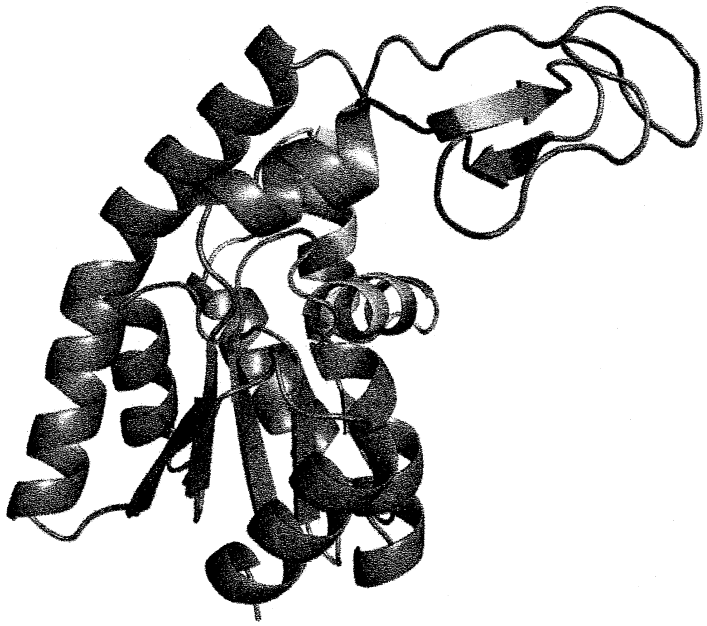

Figure 12.9 Pictorial overview of distribution of residues chosen for calculations.

^{15}N–^{1}H bond and the X axis perpendicular to the peptide bond plane. Moreover, we consider the tensor to be axially symmetric in such a frame. To interpret data, we make the simplifying assumption that the coupling potential tends to align the Z axis of the second body (i.e., of the OF frame), parallel to the direction containing the ^{15}N=^{1}H bond in the equilibrium geometry of the protein. This is reproduced by defining a frame VF having the Z axis parallel to the ^{15}N–^{1}H bond, which in general is tilted from the M_1F, where the diffusion tensor of the protein is diagonal. So, for every residue, we extracted from the geometry of the protein the set of Euler angles that transform from M_1F to VF, Ω_1. We assume that the magnetic tensors are diagonal in the same frame, that is, $\Omega_C = (0.0, 0.0, 0.0)$ degrees, and a constant tilt with respect to the OF, $\Omega_D = (0.0, 18.0, 90.0)$ degrees, following Meirovitch et al. [101].

A set of four parameters were considered adjustable and obtained via fitting: the parallel and perpendicular components of the diffusion tensor of the second body, ${}^{O}D_{1}$ and ${}^{O}D_{||}$, the strength of the axial potential, c_0^2, and a parameter called rate of exchange, R_{ex}, which gives a correction due to a very slow change in configuration of the protein [101]. Table 12.2 summarizes the values obtained for the 37 residues considered.

Figures 12.10–12.12 show the experimental and theoretical values of the T_1, T_2 and NOE at 600.0 MHz. The overall agreement is good: All the relative errors between theoretical and experimental values are within 5%. Figure 12.13 plots the values of the order parameters obtained with the standard formula

$$S = \langle \mathcal{D}^2_{0\,0}(\Omega_O) P_{eq}(\Omega_O) \rangle \tag{12.65}$$

Table 12.2 Values of Model Parameters Obtained from Fitting

Domain	Residue	${}^{O}D_{\perp}$ (10^7 Hz)	${}^{O}D_{\parallel}$ (10^{10} Hz)	R_{ex} (Hz)	c_0^2	S
AMPbd	32	1.69	10.5	2.95	2.64	0.55
	33	2.04	13.0	1.51	3.65	0.68
	36	1.55	12.7	1.38	2.82	0.58
	41	2.56	5.42	0.277	4.81	0.77
	42	2.54	4.23	0.873	4.80	0.77
	46	2.09	7.02	1.16	4.32	0.74
	48	1.38	7.27	1.30	2.50	0.53
	50	2.23	6.84	1.09	4.69	0.76
	52	2.12	7.09	0.118	4.34	0.74
	53	1.93	5.34	0.882	4.06	0.72
	55	2.36	6.55	1.01	5.13	0.78
	56	2.25	6.29	0.427	4.40	0.74
	60	2.29	5.27	0.196	5.01	0.78
CORE	2	1.29	17.7	1.60	1.77	0.39
	3	1.40	35.1	1.24	2.24	0.49
	16	1.83	11.4	4.21	3.40	0.65
	77	1.32	20.9	1.75	2.06	0.45
	86	1.69	15.6	2.38	2.70	0.56
	97	1.72	19.5	0.54	4.00	0.71
	107	1.33	28.1	2.14	1.83	0.41
	117	1.42	31.5	2.36	2.37	0.51
	170	1.63	8.95	0.898	3.47	0.66
	191	2.20	5.21	0.000	4.27	0.73
	210	1.35	25.4	1.51	3.15	0.62
LID	122	1.70	25.4	6.05	4.16	0.72
	123	1.70	12.4	2.90	3.58	0.67
	126	1.84	15.4	0.000	4.28	0.73
	132	2.58	6.59	0.000	5.38	0.80
	136	2.05	6.87	1.54	5.06	0.78
	137	2.25	6.77	0.000	5.73	0.81
	145	1.64	9.07	1.42	3.53	0.67
	151	1.35	14.7	1.20	3.09	0.62
	158	2.30	3.96	1.49	4.37	0.74
	159	1.79	8.82	0.458	4.28	0.73
P loop	8	1.84	15.4	0.161	4.33	0.74
	11	1.46	13.5	2.30	2.96	0.60

Analysis of NMR relaxation data applied to the investigation of microscopic dynamics is very promising, and a wealth of experimental measures are just waiting for advanced interpretative tools. The SRLS model is a first somewhat primitive but systematic approach which attempts to combine simplified but clearly defined physical hypotheses with a reliable physical interpretation of both dynamical and structural (through the interaction potential) properties.

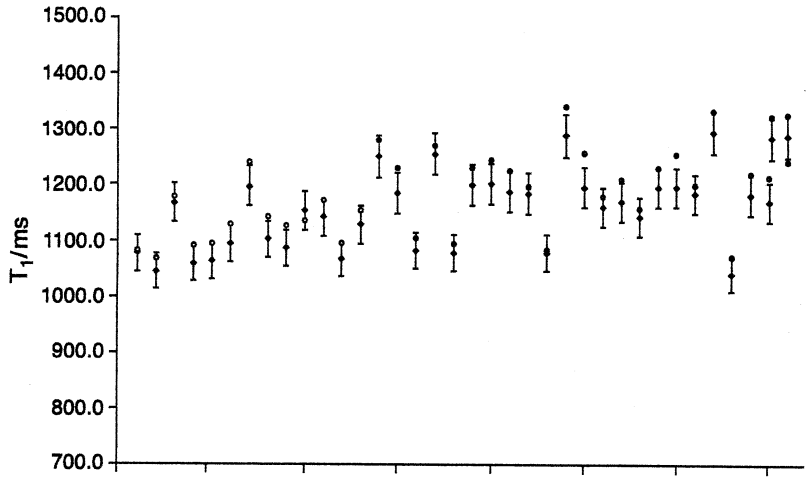

Figure 12.10 Experimental (rhombi) and theoretical (circles) T_1 values at 600.0 MHz.

12.4 CONCLUSIONS

Stochastic models are a comprehensive and mature tool for interpreting molecular relaxation phenomena observed from magnetic resonance spectroscopies. Modern implementations [104, 105] allow one to exploit the modularity of numerical algorithms to obtain highly efficient software tools which can tackle diverse molecular systems, especially in connection with QM determination of structural and dynamical properties of complex molecular systems. The future of stochastic approaches can be thought of in connection with the proper development of

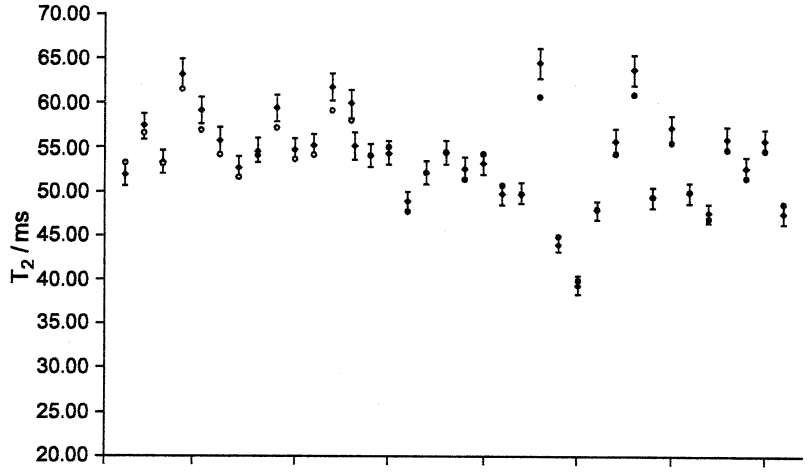

Figure 12.11 Experimental (rhombi) and theoretical (circles) T_2 values at 600.0 MHz.

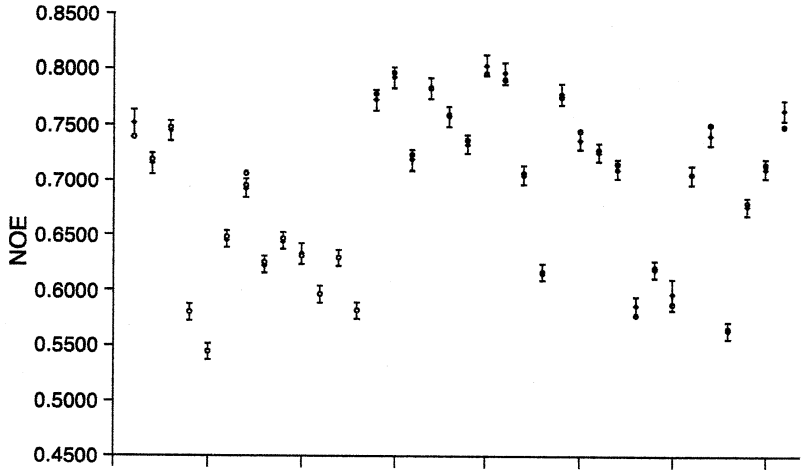

Figure 12.12 Experimental (rhombi) and theoretical (circles) NOE values at 600.0 MHz.

multiscale approaches. Indeed, in the near future one can envision integrated mesoscopic–atomistic methods which combine stochastic modeling of slow, or "soft," variables and appropriate treatment (at a molecular dynamics level) for fast, or "hard," degrees of freedom. This methodology would be ideal to treat large flexible biomolecules, allowing an economical computational treatment. Moreover, foundations of stochastic many-body approaches can be based on atomistic-derived descriptions, rendering these augmented treatments predictive in nature; data fitting could then be seen as a refining step geared toward overcoming errors in parameter evaluation implied by the approximations inherent in the various components of the protocol.

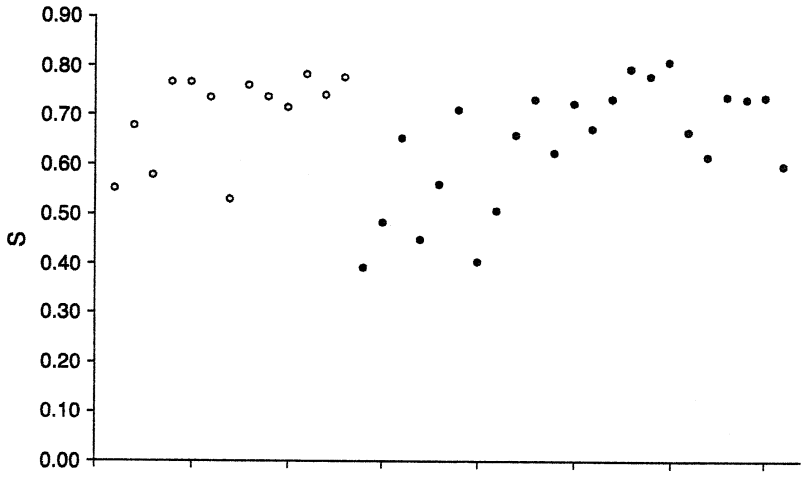

Figure 12.13 Order parameters obtained from fitting.

REFERENCES

1. Y. E. Ryabov, C. Geragthy, A. Varshney, D. Fushman, *J. Am. Chem. Soc.* **2006**, *128*, 15432.
2. D. J. Schneider, J. H. Freed, *Adv. Chem. Phys.* **1989**, *73*, 387.
3. M. Balog, T. Kálai, J. Jeko, Z. Berente, H. J. Steinhoff, M. Engelhard, K. Hideg, *Tetrahedron Lett.* **2003**, *44*, 9213.
4. W. L. Hubbell, H. S. Mchaourab, C. Altenbach, M. Lietzow, *Structure 1996 4*, **1996**.
5. H. J. Steinhoff, *Front. Biosci.* **2002**, *7*, 2002.
6. Z. Zhang, M. R. Fleissner, D. S. Tipikin, Z. Liang, J. K. Moscicki, K. A. Earle, W. L. Hubbell, J. H. Freed, *J. Phys. Chem. B* **2010**, *114*, 5503.
7. V. S. S. Sastry, A. Polimeno, R. H. Crepeau, J. H. Freed, *J. Chem. Phys.* **1996**, *107*, 5753.
8. V. S. S. Sastry, A. Polimeno, R. H. Crepeau, J. H. Freed, *J. Chem. Phys.* **1996**, *107*, 5773.
9. A. Polimeno, J. H. Freed, *J. Phys. Chem.* **1995**, *99*, 10995.
10. P. P. Borbat, A. J. Costa-Filho, K. A. Earle, J. K. Moscicki, J. H. Freed, *Science* **2001**, *291*, 266.
11. M. Ge, J. H. Freed, *Biophys. J.* **2009**, *96*, 4925.
12. Y.-W. Chiang, A. J. Costa, J. H. Freed, *J. Phys. Chem. B* **2007**, *111*, 11260.
13. M. J. Swamy, L. Ciani, M. Ge, A. K. Smith, D. Holowka, B. Baird, J. H. Freed, *Biophys. J.* **2006**, *90*, 4452.
14. S. Van Doorslaer, E. Vinck, *Phys. Chem. Chem. Phys.* **2007**, *9*, 4620.
15. O. Schiemann, T. F. Prisner, *Q. Rev. Biophys.* **2007**, *40*, 1.
16. P. P. Borbat, J. H. Freed, Measuring distances by pulsed dipolar ESR spectroscopy: spin-labeled histidine kinases, in *Two-Component Signaling Systems, Part B*, M. Simon, B.R. Crane, A.B. Crane, Eds., Methods in Enzymology 423, Ch. 3, 2007, pp. 52–116.
17. P. Borbat, H. Mchaourab, J. Freed, *J. Am. Chem. Soc.* **2002**, *124*, 5304.
18. A. J. Costa-Filho, Y. Shimoyama, J. H. Freed, *Biophys. J.* **2003**, *84*, 2619.
19. G. Jeschke, Y. Polyhach, *Phys. Chem. Chem. Phys.* **2007**, *9*, 1895.
20. F. Tombolato, A. Ferrarini, J. H. Freed, *J. Phys. Chem. B* **2006**, *110*, 26248.
21. F. Tombolato, A. Ferrarini, J. H. Freed, *J. Phys. Chem. B* **2006**, *110*, 26260.
22. A. Polimeno, M. Zerbetto, L. Franco, M. Maggini, C. Corvaja, *J. Am. Chem. Soc.* **2006**, *128*, 4734.
23. V. Barone, M. Brustolon, P. Cimino, A. Polimeno, M. Zerbetto, A. Zoleo, *J. Am. Chem. Soc.* **2006**, *128*, 15865.
24. M. Zerbetto, S. Carlotto, A. Polimeno, C. Corvaja, L. Franco, C. Toniolo, F. Formaggio, V. Barone, P. Cimino, *J. Phys. Chem. B* **2007**, *111*, 2668.
25. P.-O. Westlund, H. Wennerstrom, *Phys. Chem. Chem. Phys.* **2010**, *12*, 201.
26. S. K. Misra, *J. Mag. Res.* **2007**, *189*, 59.
27. A. Borel, R. B. Clarkson, R. L. Belford, *J. Chem. Phys.* **2007**, *126*, 054510.
28. M. Lindgren, A. Laaksonen, P.-O. Westlund, *Phys. Chem. Chem. Phys.* **2009**, *11*, 10368.
29. D. Sezer, J. H. Freed, B. Roux, *J. Am. Chem. Soc.* **2009**, *131*, 2597.
30. A. Polimeno, J. H. Freed, *Adv. Chem. Phys.* **1993**, *83*, 89.
31. A. Arcioni, C. Bacchiocchi, L. Grossi, A. Nicolini, C. Zannoni, *J. Phys. Chem. B* **2002**, *206*, 9245.

32. A. Nayeem, S. Rananavare, V. Sastry, J. Freed, *J. Chem. Phys.* **1992**, *96*, 3912.
33. J. Moscicki, Y. Shin, J. Freed, *J. Chem. Phys.* **1993**, *99*, 634.
34. A. Arcioni, C. Bacchiocchi, I. Vecchi, G. Venditti, C. Zannoni, *Chem. Phys. Lett.* **2004**, *396*, 433.
35. J. H. Freed, *Electron Spin Relaxation in Liquids*, Plenum, New York, 1972.
36. R. Kubo, *J. Math. Phys.* **1963**, *4*, 174.
37. R. Kubo, *J. Phys. Soc. Jpn. Suppl.* **1969**, *26*, 1.
38. W. Wassam, J. Freed, *J. Chem. Phys.* **1982**, *76*, 6133.
39. W. Wassam, J. Freed, *J. Chem. Phys.* **1982**, *76*, 6150.
40. Y. Tanimura, *J. Phys. Soc. Jpn.* **2006**, *75*, 082001.
41. V. Barone, *J. Chem. Phys.* **1994**, *101*, 10666.
42. V. Barone, *Theor. Chem. Acc.* **1995**, *91*, 113.
43. V. Barone, *Advances in Density Functional Theory. Part I,* Vol. 287, World Science, Singapore, 1995.
44. R. Improta, V. Barone, *Chem. Rev.* **2004**, *104*, 1231.
45. D. Feller, E. R. Davidson, *J. Chem. Phys.* **1988**, *88*, 5770.
46. S. A. Perera, L. M. Salemi, R. J. Bartlett, *J. Chem. Phys.* **1997**, *106*, 4061.
47. A. R. Al Derzi, S. Fau, R. J. Bartlett, *J. Phys. Chem. A* **2003**, *107*, 6656.
48. H. M. McConnell, *J. Chem. Phys.* **1963**, *39*, 1910.
49. H. M. McConnell, *Proc. R. A. Welch Found. Conf. Chem. Res.* **1967**, *11*, 144.
50. A. J. Stone, *Mol. Phys.* **1964**, *7*, 311.
51. C. Adamo, V. Barone, R. Subra, *Theor. Chem. Acco. Theory Comput. Model. (Theor. Chim. Acta)* **2000**, *104*, 207.
52. F. Neese, *J. Chem. Phys.* **2001**, *115*, 11080.
53. R. Ditchfield, *Mol. Phys.* **1974**, *27*, 789.
54. J. R. Cheeseman, G. W. Trucks, T. A. Keith, M. J. Frisch, *J. Chem. Phys.* **1996**, *104*, 5497.
55. O. L. Malkina, J. Vaara, B. Schimmelpfennig, M. Munzarova, V. G. Malkin, M. Kaupp, *J. Am. Chem. Soc.* **2000**, *122*, 9206.
56. I. Ciofini, C. Adamo, V. Barone, *J. Chem. Phys.* **2004**, *121*, 6710.
57. V. Barone, R. Subra, *J. Chem. Phys.* **1996**, *104*, 2630.
58. F. Jolibois, J. Cadet, A. Grand, R. Subra, N. Rega, V. Barone, *J. Am. Chem. Soc.* **1998**, *120*, 1864.
59. V. Barone, P. Carbonniere, C. Pouchan, *J. Chem. Phys.* **2005**, *122*, 224308.
60. J. A. Nillson, L. A. Eriksson, A. Laaksonen, *Mol. Phys.* **2001**, *99*, 247.
61. M. Nonella, G. Mathias, P. Tavan, *J. Phys. Chem. A* **2003**, *107*, 8638.
62. J. R. Asher, N. L. Doltsinis, M. Kaupp, *Magn. Reson. Chem.* **2005**, *43*, S237.
63. M. Pavone, C. Benzi, F. De Angelis, V. Barone, *Chem. Phys. Lett.* **2004**, *395*, 120.
64. M. Pavone, P. Cimino, F. De Angelis, V. Barone, *J. Am. Chem. Soc.* **2006**, *128*, 4338.
65. M. Pavone, A. Sillanpaa, P. Cimino, O. Crescenzi, V. Barone, *J. Phys. Chem. B* **2006**, *110*, 16189.
66. S. Koseki, M. W. Schmidt, M. S. Gordon, *J. Phys. Chem.* **1992**, *96*, 10768.
67. E. Fermi, *Zeits. Phy. A Hadrons Nuclei* **1930**, *60*, 320.

68. R. A. Frosch, H. M. Foley, *Phys. Rev.* **1952**, *88*, 1337.
69. J. Tomasi, B. Mennucci, R. Cammi, *Chem. Rev.* **2005**, *105*, 2999.
70. V. Barone, M. Cossi, J. Tomasi, *J. Chem. Phys.* **1997**, *107*, 3210.
71. C. Benzi, M. Cossi, R. Improta, V. Barone, *J. Comp. Chem.* **2005**, *26*, 1096.
72. M. Cossi, G. Scalmani, N. Rega, V. Barone, *J. Chem. Phys.* **2002**, *117*, 43.
73. V. Barone, A. Polimeno, *Phys. Chem. Chem. Phys.* **2006**, *8*, 4609.
74. V. Barone, A. Grand, C. Minichino, R. Subra, *J. Chem. Phys.* **1993**, *99*, 6745.
75. V. Barone, C. Adamo, Y. Brunel, R. Subra, *J. Chem. Phys.* **1996**, *105*, 3168.
76. V. Barone, *Chem. Phys. Lett.* **1996**, *262*, 201.
77. M. Pavone, C. Benzi, F. D. Angelis, V. Barone, *Chem. Phys. Lett.* **2004**, *395*, 120.
78. O. Crescenzi, M. Pavone, F. de Angelis, V. Barone, *J. Phys. Chem. B* **2005**, *109*, 445.
79. G. Moro, *Chem. Phys.* **1987**, *118*, 181.
80. H. Yamakawa, *J. Chem. Phys.* **1970**, *53*, 436.
81. J. Rotne, S. Prager, *J. Chem. Phys.* **1969**, *50*, 4831.
82. E. Meirovitch, D. Igner, E. Igner, G. Moro, J. H. Freed, *J. Chem. Phys.* **1982**, *77*, 3915.
83. G. Moro, J. H. Freed, *J. Chem. Phys.* **1981**, *74*, 3757.
84. G. Moro, J. H. Freed, *Large-Scale Eigenvalue Problems, Mathematical Studies Series*, Vol. 127, Elsevier, New York, 1986.
85. H. J. Hogben, P. J. Hore, I. Kuprov, *J. Chem. Phys.* **2010**, *132*, 174101.
86. M. A. Morsy, G. A. Oweimreen, J. S. Hwang, *J. Phys. Chem.* **1996**, *100*, 8331.
87. C. Benzi, M. Cossi, V. Barone, *J. Chem. Phys.* **2005**, *123*, 194909.
88. C. Adamo, V. Barone, *J. Chem. Phys.* **1999**, *110*, 6158.
89. S. Chandrasekhar, *Liquid Crystals*, 2nd ed., University Press, Cambridge, 1992.
90. P. G. De Gennes, J. Prost, *The Physics of Liquid Crystals*, 2nd ed., Oxford University Press, New York, 1993.
91. G. Vertogen, W. H. de Jeu, *Thermotropic Liquid Crystals, Fundamentals*, Springer-Verlag, Berlin, 1993.
92. F. M. Leslie, *Quart. J. Mech. Appl. Math.* **1966**, *19*, 357.
93. F. M. Leslie, *Adv. Liq. Cryst.* **1979**, *4*, 1.
94. J. L. Ericksen, *Trans. Soc. Rheol.* **1961**, *5*, 23.
95. J. L. Ericksen, *Adv. Liq. Cryst.* **1976**, *2*, 233.
96. A. G. PalmerIII, *Annu. Rev. Biophys. Biomol. Struct.* **2001**, *20*, 129.
97. G. Lipari, A. Szabo, *J. Am. Chem. Soc.* **1982**, *104*, 4546.
98. G. Lipari, A. Szabo, *J. Am. Chem. Soc.* **1982**, *104*, 4559.
99. K. A. Earle, J. K. Moscicki, A. Polimeno, J. H. Freed, *J. Chem. Phys.* **1997**, *106*, 9996.
100. Y. E. Shapiro, E. Kahana, V. Tugarinov, Z. Liang, J. H. Freed, E. Meirovitch, *Biochemistry* **2002**, *41*, 6271.
101. E. Meirovitch, A. Polimeno, J. H. Freed, *J. Phys. Chem. B* **2006**, *110*, 20615.
102. E. Meirovitch, A. Polimeno, J. H. Freed, *J. Phys. Chem. B* **2007**, *111*, 12865.
103. A. Abragam, *The Principles of Nuclear Magnetism*, Oxford University Press, London, 1961.
104. M. Zerbetto, A. Polimeno, V. Barone, *Comput. Phys. Comm.* **2009**, *180*, 2680.
105. M. Zerbetto, A. Polimeno, E. Meirovitch, *J. Phys. Chem. B* **2009**, *113*, 13613.

INDEX

Computational Strategies for Spectroscopy: From Small Molecules to Nano Systems, First Edition. Edited by Vincenzo Barone.